

Abstract: Gain of aromaticity or relief of antiaromaticity along a reaction path are important factors to consider in mechanism studies. Analysis of such changes along potential energy surfaces has historically focused on reactions in the electronic ground state (S_0), but can also be used for excited states. In the lowest $\pi\pi^*$ states, the electron counts for aromaticity and antiaromaticity follow Baird's rule where $4n$ π -electrons indicate aromaticity and $4n+2$ π -electrons antiaromaticity. Yet, there are also cases where Hückel's rule plays a role in

the excited state. The electron count reversals of Baird's rule compared to Hückel's rule explain many altered physico-chemical properties upon excitation of (hetero)annulene derivatives. Here we illustrate how the gain of excited-state aromaticity (ESA) and relief of excited-state antiaromaticity (ESAA) have an impact on photoreactivity and photostability. Emphasis is placed on recent findings supported by the results of quantum chemical calculations, and photoreactions in a wide variety of areas are covered.

1. Introduction

Upon absorption of light of an appropriate wavelength, a molecule becomes excited to its lowest electronically excited state. In this state, the molecular properties can change drastically compared to the S_0 state. For example, some bonds that were single bonds in the S_0 state get double bond character, and vice versa. The dipole moment and the pK_a value can also change upon excitation. In essence, the molecule becomes "a different molecule" as a result of the altered electronic structure in the excited state. To predict what changes take place, qualitative models and concepts can be immensely useful, yet, while there is a plethora of such "fuzzy" concepts for the S_0 state,^[1] they are much less common for the lowest electronically excited states where photochemical reactions occur. Such qualitative tools are more intricate to develop, although there are already work towards descriptions that allow for qualitative understanding of electronically excited states with a basis in high-level quantum chemical computations.^[2,3] In parallel, one may also explore to what extent existing qualitative concepts for the S_0 state can be expanded and reformulated to excited states. Herein, we largely follow the second line.

Aromaticity and antiaromaticity are two "fuzzy" chemical concepts with widespread usage in the S_0 state.^[4–9] It has, for example, been estimated that about two thirds of all known molecules are aromatic or have aromatic components.^[6] The first of these concepts explains the high stability and inert reactivity of $[4n+2]$ annulenes in their S_0 states while the second is reflected in the instability and enhanced reactivity of many $[4n]$ annulenes. However, in the lowest $\pi\pi^*$ states the electron count rules for aromaticity and antiaromaticity are reversed, which means that $[4n+2]$ annulenes are antiaromatic while $[4n]$ annulenes are aromatic. Nowadays, this relationship is referred to as Baird's rule.^[10–18]

Studies which apply excited-state aromaticity and antiaromaticity (in short, excited-state (anti-)aromaticity, ES(A)A) to rationalize photoreactivity outside the area of pericyclic photochemical reactions are still rather limited although the number of such studies starts to increase. Yet, based on the importance of the aromaticity and antiaromaticity in the S_0 state we argue that they may also be widely applicable within photochemistry.


In order to address the importance and usefulness of the ES(A)A concepts to organic photochemistry, we now summarize how they relate to the photoreactivity and photostability of a series of π -conjugated species and their specific photochemical transformations. Significant focus is given to photochemical observations made during the last eight years (the time since our two previous reviews),^[13,14] although we also discuss earlier studies. An emphasis is placed on studies in which experimental findings are supported by results from quantum chemical computations on changes in ES(A)A along the reaction pathway. Through a review of recent studies in which the effects of ES(A)A on photoreactivity are addressed we argue that the general applicability of the concepts becomes more apparent, which can trigger further research and applications in this revived area of organic photochemistry. This provides for the development of novel (anti-)aromatic chemistry in excited states. Before briefly discussing the historic development of the field, we give a short summary of computational tools for excited-state (anti-)aromaticity assessments including their weaknesses. Yet, the main part of the paper is focused on photoreactions that involve gain of ESA or relief of ESAA.


[a] Dr. J. Yan, Dr. T. Slanina, Prof. Dr. H. Ottosson
Department of Chemistry-Ångström Laboratory
Uppsala University
Box 523, 751 20 Uppsala (Sweden)
E-mail: henrik.ottosson@kemi.uu.se

[b] Dr. T. Slanina
Institute of Organic Chemistry and Biochemistry of the
Czech Academy of Sciences
Flemingovo náměstí 2, 16610 Prague 6 (Czech Republic)

[c] J. Bergman
Medicinal Chemistry
Research and Early Development Cardiovascular, Renal and Metabolism
BioPharmaceuticals R&D, AstraZeneca
Gothenburg (Sweden)

 This publication is part of a Special Collection on aromatic chemistry in collaboration with the "19th International Symposium on Novel Aromatic Compounds (ISNA-19)".

 Selected by the Editorial Office for our Showcase of outstanding Review-type articles (www.chemeurj.org/showcase).

 © 2023 The Authors. Chemistry - A European Journal published by Wiley-VCH GmbH. This is an open access article under the terms of the Creative Commons Attribution License, which permits use, distribution and reproduction in any medium, provided the original work is properly cited.

2. Computational Assessments of Excited-State (Anti)aromaticity

A brief overview of the theoretical and computational aspects of aromaticity and antiaromaticity concepts is crucial as a background to excited-state aromaticity and antiaromaticity. The aromaticity research area has grown rapidly in recent years with a large number of novel and unusual forms of aromaticity,^[9,19] sometimes vigorously debated. Debated is also which aspect of aromaticity should be emphasized (the energetic, magnetic, geometric or electronic, Figure 1) and which computational and experimental descriptors should be used. Our recommendation is that assessments should be based on as wide a variety of descriptors as possible so that they together represent the different aspects of aromaticity. In this context, it should be noted that aromaticity and antiaromaticity are far from settled concepts, and that the causes need further fundamental explorations leading to alternative and deepened descriptions.^[20–22]

It should be noted that for excited states there is no present experimental technique for aromaticity assessments analogous to ¹H NMR spectroscopy for the S₀ state. Experimental

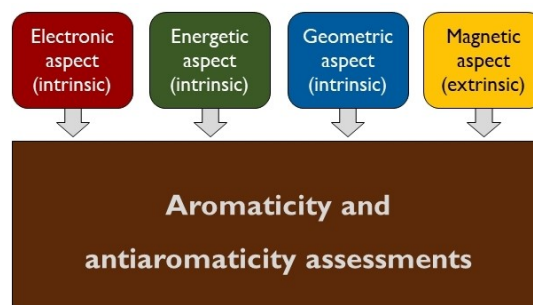
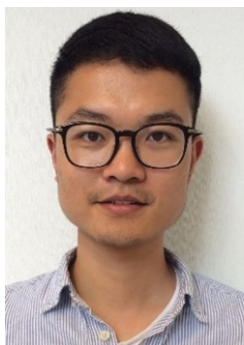


Figure 1. The four different aspects of aromaticity and antiaromaticity that should be considered in the assessment of the (anti-)aromatic character of a molecule, and categorization of the aspects as intrinsic or extrinsic properties.

observations that potentially are linked to excited-state (anti-)aromaticity must therefore be supported by results from quantum chemical computations of various aromaticity indices as comprehensively as possible. In addition, the computational findings should as far as possible be rationalized through qualitative theory; is the investigated ring Baird aromatic in the

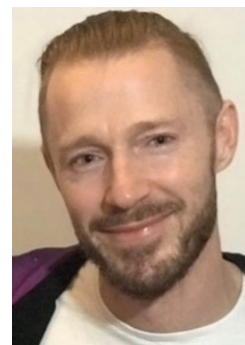
Jiajie Yan finished his PhD (2017) in organic chemistry at Uppsala University (Sweden), specializing in the development of synthetic regenerable chalcogenide antioxidants. Then he worked as a postdoc (2018–2019) at the University of Manchester (UK). There, he focused on material-oriented synthetic sulfur chemistry. Later, he did a two-year postdoc (2019–2021) with Assoc. Prof. Henrik Ottosson on photochemical transformations of (hetero-)aromatics back at Uppsala University. Currently, Jiajie is working as a senior research scientist at TdB Labs AB.



Tomáš Slanina received his Ph.D. in organic chemistry in 2015 jointly from Masaryk University (Brno, Czech Republic) and the University of Regensburg (Germany), under the supervision of Profs. Petr Klán and Burkhard König. He later worked as a postdoctoral researcher with Profs. Alexander Heckel at Goethe University (Frankfurt am Main, Germany) and Henrik Ottosson at Uppsala University (Sweden). He is currently a Redox Photochemistry group leader at the Institute of Organic Chemistry and Biochemistry in Prague (Czech Republic). His research interests include organic chemistry, photochemistry, physical organic chemistry, electrochemistry, transient and steady-state spectroscopy, studying reaction mechanisms, and chemical biology.



Joakim Bergman received his MSc in chemistry at the University of Linköping (Sweden) in 2001. He directly accepted an offer to join AstraZeneca, where he is still active. Besides medicinal chemistry, Joakim is an expert in small-molecule synthesis. Furthermore, he is experienced in lipid chemistry, macrocycle- and oligonucleotide conjugate synthesis. He has been very active in academic collaborations (~10 publications), many within the area of photochemistry and photo-redox catalysis. In 2015, he received (globally and internally) the AstraZeneca Senior Scientist of the Year Award.



Henrik Ottosson received his PhD in 1996 (University of Gothenburg, Sweden) on quantum chemical calculations of NMR chemical shifts. As a postdoc in the group of Prof. Josef Michl (University of Colorado at Boulder, USA) he explored σ -conjugated oligosilanes spectroscopically and computationally. He started his group at Uppsala University in 2000 within organosilicon chemistry, and became Assoc. Prof. in Physical Organic Chemistry in 2003. His research today focuses on organic photochemistry, where he is an international leader on excited-state (anti-)aromaticity. He is also active within urban science and recently coordinated the Urban Sustainability initiative within the Uppsala University Sustainability Initiatives.



excited state, or is it Hückel aromatic? Several pitfalls of the ESA and ESAA concepts exist, and a combination of quantitative quantum chemical computations with qualitative molecular orbital (MO) or valence bond (VB) theory often allows one to avoid these.

One can also argue on which quantum chemical method the aromaticity assessments should be based; a wavefunction or a density functional theory (DFT) method, and questions come up related to the single- or multiconfigurational character of a certain state, or if a functional which includes long-range corrections is crucial. Obviously, aromaticity effects of states with multiconfigurational character must be computed with relevant methods (e.g., CASSCF). In this regard, singlet excited states are usually more difficult to compute than triplet states as the former often are more multiconfigurational. This also affects calculations of aromaticity indices of singlet excited states, for example, nucleus independent chemical shifts (NICSs) calculated with CASSCF are strongly recommended over those obtained using an anti-Aufbau DFT approach.^[23] In DFT calculations there is also the question on the choice of functional as there can be substantial variations in the degree of Baird aromaticity for large and macrocyclic molecules.^[24–26] Finally, there is a larger portfolio of aromaticity descriptors available for T_1 states than for S_1 states as the former can be performed with regular Kohn-Sham DFT whereby nearly the same portfolio of descriptors exists as for the S_0 state. In contrast, the S_1 state must rely on time-dependent DFT (TD-DFT).

Magnetic aromaticity descriptors have traditionally had a central position since evidence for diatropic (aromatic) ring currents are easily gathered experimentally through NMR spectroscopy. Accordingly, there are a number of computational approaches for the analysis of the induced current densities and related properties of a molecule when placed in a magnetic field. For the assessments of the magnetic aspects of aromaticity, the anisotropy of the induced current density (ACID) is presently used intensively.^[27] Yet, methods for computations of magnetically induced current density maps have become gradually more available.^[28,29] Here, it is notable that the ACID approach has drawbacks as it only builds on the symmetric tensor components, and the anisotropy of the full tensor (anisotropy of the asymmetric magnetically induced current density (AACID)) captures features neglected by ACID, and it changes in a more regular way with bond lengths of a few prototypical aromatic molecules.^[30] The NICS methodology,^[31] which today exist in a number of versions,^[32–34] is the most widely used aromaticity index. It has been recommended to use the zz-tensor component of the shielding 1.0 Å above the ring plane, abbreviated as NICS(1)_{zz}.^[32] Yet, for polycyclic molecules it is strongly discouraged to rely on NICS(1)_{zz} computations at centers of individual rings as this overlooks that NICS values in such compounds are composites with contributions from several induced current circuits, for example, in S_0 anthracene from 6π -, 10π - and 14π -electron circuits.^[35] For polycyclic molecules the NICS-XY scan approach should instead be used as it allows for identification of both local and global ring currents.^[34] As there is no simple one-to-

one relationship between NICS and induced current density maps it is often advisable to compute also the latter.^[36] On the other hand, bond currents can be derived from NICS values.^[37,38]

Yet, the molecular response to the perturbing magnetic field (the current densities) only exists when the molecule is situated in the applied magnetic field. Thus, properties related to the magnetic aspect of (anti-)aromaticity (e.g., bond currents and NICS) are extrinsic properties. The current densities are molecular responses which can be described through virtual electronic transitions,^[21] yet, together with geometric and spectroscopic aspects the magnetic aspect has been considered as secondary relative to the energetic aspect which stem from cyclic electron delocalization.^[39] Indeed, there are molecules for which the magnetic descriptors deviate substantially from the results of other aromaticity descriptors.^[39,40]

The three other aspects of aromaticity (geometric, electronic and energetic) relate solely to the electron configuration of the electronic state in focus. They do not vary with external perturbations, and are thus intrinsic properties (Figure 1). The geometric aspect of aromaticity is often assessed by using the harmonic oscillator model of aromaticity (HOMA),^[41] which, however, relies on parameters for the S_0 state, and accordingly, should be used with care for excited states.

Several electronic indices exist,^[42] including the multicenter index (MCI),^[43] the aromatic fluctuation index (FLU),^[44,45] and the electron density of delocalized bonds (EDDB) method.^[46] Also, properties of the π -component of the electron localization function (ELF) has been used.^[47,48] The MCI index reflects the simultaneous sharing of electrons between all atoms in a cycle, yet, it can only be used for small to medium-sized rings (fewer than 12 atoms) as it considers permutations of all electrons between the atoms in a ring. These drawbacks are addressed by the AV₁₂₄₅ index.^[49] FLU gives a measure of uniformity of the electron delocalization around a cyclic molecule and its bonding differences with respect to an aromatic reference which is a stable compound, and thus, it cannot be applied to transition states and structures far from the reference. Finally, EDDB is a more newly developed index which builds on the bond-order projection formalism to decompose the molecular electron density into three parts; into electrons localized on atoms, those localized between atom pairs, and those delocalized between conjugated bonds. With regard to excited states, it should be noted that values of electronic indices computed with KS-DFT are different from those computed with TD-DFT. Thus, MCI values computed at UDFT level for molecules in their T_1 states cannot be compared to MCI values for the S_1 states of the same molecules computed with TD-DFT. To compare, the MCI values of the T_1 state must be computed also at TD-DFT level. Noteworthy, both MCI and FLU can be separated into π_α - and π_β -spin components, which is often useful for the proper assessment of triplet state Baird aromaticity.^[50,51]

The energetic aromaticity aspects can be determined through isodesmic or homodesmotic reactions, yet, today the isomerization stabilization energy (ISE) is often used as it can circumvent perturbing structural factors, for example, strain and presence of heteroatoms.^[52–55] In this approach, either the energy differences between monomethylated annulenes and

their nonaromatic isomers with exocyclic methylene groups are determined (labeled ISE type I (ISE_I)), or the energy differences between indene and the nonaromatic isoindene isomer (labeled ISE_{II}) are determined. The ISE method can, however, be problematic for excited states. For example, the lowest excited state of the nonaromatic isomer may not be the state which is best related to the lowest excited state of the (anti-)aromatic isomer, and this is especially the case for singlet excited states. For triplet states, on the other hand, the nonaromatic isomer being a linear polyene may twist the exocyclic C=C bond. Both effects lead to ambiguities in the assessment of the energetic aspect of excited-state (anti-)aromaticity.

In addition to being computationally more challenging, excited-state (anti-)aromaticity also comes with the alert that aromaticity in an excited state is not necessarily Baird aromaticity; there are molecules which are Hückel aromatic in their excited states,^[56–58] and there are those with excited states that are Hückel- and Baird-aromatic hybrids.^[50,51] Finally, similar to the hexagonal hydrogen-bonded (HF)₃ trimer, some transition-metal cycles and carborane-fused heterocycles in the S₀ state,^[59–62] one can encounter situations in excited states where negative NICS values are found in the center of rings without diatropic ring currents. Instead, localized circulations at the edges, or paratropic ring currents in adjacent rings, can lead to a negative NICS value in a certain ring. Thus, it is important to explore alternative rationalization models for the computed results at hand for a specific compound; there may be other causes for the observed results than that the compound is Baird aromatic.

Taken together, for the proper assessment of excited-state aromaticity and antiaromaticity, caution should be exercised before one comes to the conclusion that a certain molecule is (Baird-) aromatic or antiaromatic in its lowest excited states. There are issues on whether a correct quantum chemical method has been chosen for the electronic state under consideration, there are also issues related to the aromaticity descriptors, and finally, one should as far as possible derive and test alternative ways to rationalize the computational results observed (Figure 2).

3. Brief History of Excited-State (Anti-)aromaticity

Hückel's $4n+2$ rule tells that annulenes, that is, fully π -conjugated all-carbon monocycles, with $4n+2$ π -electrons are aromatic in their closed-shell S₀ state.^[63] In contrast, annulenes with $4n$ π -electrons are antiaromatic, a concept introduced by Breslow.^[64] Moving to electronically excited states, in the mid-60s Dewar^[65,66] and Zimmerman^[67] independently analyzed pericyclic reactions (both thermal and photochemical ones) by linking allowed and forbidden such reactions to transition state (TS) aromaticity and antiaromaticity, respectively. They also concluded that the electron counts for aromaticity and antiaromaticity in the first $\pi\pi^*$ excited states are opposite to those given for the S₀ state. The generality in the aromaticity

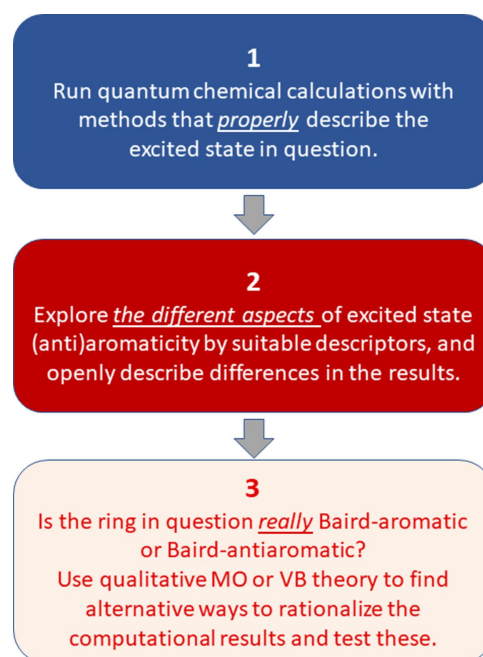


Figure 2. The three steps that should be followed for a comprehensive investigation of aromaticity and antiaromaticity effects in electronically excited states and triplet ground states.

and antiaromaticity reversal of the lowest $\pi\pi^*$ states when compared to the S₀ state was revealed by Baird in 1972 when he used perturbation molecular orbital theory to show this for the lowest $\pi\pi^*$ triplet state (T₁).^[10] The rules for Baird aromaticity and antiaromaticity in the lowest $\pi\pi^*$ triplet state can be understood through π -orbital energy changes upon fusion of two polyenyl radical fragments to an annulene in its lowest triplet state (for further reading see refs. [10], [13] and [17]).

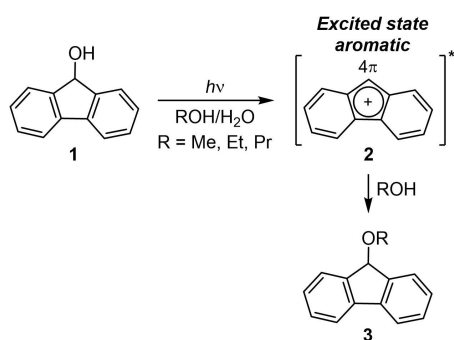
Addressing photoreactivity, Baird wrote that “the antiaromaticity associated with the triplet state of benzenoid hydrocarbons is predicted to yield drastic changes in the intermolecular reactivity compared to the ground state.”^[10] A few years later, Aihara, when analyzing the resonance energies from the Hückel MO theory of annulenes with either Hückel- or Möbius-orbital topology in the first $\pi\pi^*$ state, concluded that “either conformation of any annulene in the excited state can be predicted to have an aromatic character opposite to that in the ground state”.^[68] Note that the change in aromatic to antiaromatic character, or vice versa, when changing the number of π -electrons ($4n$ vs. $4n+2$), the orbital topology (Hückel vs. Möbius), or electronic state (π^2 vs. $\pi\pi^*$) can be summarized in a cube mnemonic.^[19] Aihara also approached photoreactivity, writing that “the resonance energy [of benzene] becomes greatly negative when [benzene] is electronically excited. Such a situation is best represented by a high reactivity of this compound in the excited state.”

In 1998, Schleyer and co-workers, using high-level quantum chemical calculations, analyzed a variety of properties, including nucleus independent chemical shifts (NICS's), of small

[4n]annulenes in their lowest triplet states.^[69] Among the species analyzed, they found that the cyclopentadienyl cation is Baird aromatic in its triplet ground state (T_0), a species earlier explored through EPR spectroscopy by Saunders et al. and observed experimentally to have a T_0 state with a highly symmetric pentagonal structure.^[70] Using valence bond (VB) theory, Zilberg and Haas showed, also in 1998, that a triplet state [4n]annulene can be viewed as a Hückel-aromatic [4n–2]annulene dication plus two non-bonded same-spin π -electrons.^[71] Later, the (anti-)aromaticity of small annulenes in their S_1 states have been analyzed computationally based on magnetic and electronic criteria, indicating that Baird's rule is often also applicable to these states.^[72–75] For the T_1 state, it has further been found that [4n]annulenes are stabilized while [4n + 2]annulenes are destabilized relative to nonaromatic references,^[54,55] findings that should be reflected in the shapes of T_1 state potential energy surfaces (PESs), thus influencing photoreactions that proceed in this state.

From the experimental aspect, Wan and co-workers pioneered the application of the excited-state aromaticity concept outside the area of pericyclic photoreactions.^[76–88] In 1985, they revealed facile photosolvolytic of 9-fluorenone (1) in methanol (Scheme 1), and concluded that the driving force is “the formation of an aromatic 4 π cationic system in the excited state”.^[76] Subsequently, his group investigated the photochemical implications of the ESA concept applied to photoacidity and photobasicity, and to photodecarboxylations. They also provided the first spectroscopic evidence for the gain of excited-state aromatic character when they observed a large Stokes shift in dibenz[b,f]oxepin (4) and, based on simple π -SCF PPP calculations, linked this to the attainment of a cyclically conjugated 8 π -electron cycle in the S_1 state.^[87] Much later, quantum chemical calculations of 8 π -electron heterocycles by Toldo et al. further confirmed the photoinduced geometrical planarization and gain of Baird aromaticity in the S_1 and also the T_1 states.^[89]

The excited-state aromaticity concept was also found to be important for “aromatic chameleon” compounds, that is, compounds that can adapt to the different aromaticity rules in different electronic states.^[90] Fulvenes are aromatic chameleon compounds which are dipolar in their S_0 , S_1 and T_1 states, yet in opposite directions in the S_1 and T_1 states compared to the S_0



Scheme 1. Photochemical solvolysis of 9-fluorenone (1) with an excited-state Baird-aromatic 4 π -electron cationic intermediate (2).

state as a consequence of the electron count reversals in the aromaticity rules (Figure 3A). That is, in the ground state the five-membered ring is influenced by 6 π -electron Hückel aromaticity while in the lowest $\pi\pi^*$ states this ring adopts some 4 π -electron Baird aromaticity. As an effect of the aromaticity/antiaromaticity switch and a resulting reversal in the dipole moment, the excitation energies to the S_1 and T_1 states are tunable through introduction of electron-donating or electron-withdrawing substituents at the exocyclic C atom or at the ring that either stabilize or destabilize the excited states as exemplified by fulvenes 5–8 (Figure 3B).^[91,92] The T_1 state energies were shown to correlate well with changes in various aromaticity indices upon excitation from S_0 to T_1 , for example, $\Delta NICS(1)_{ZZ,S-T}$, $\Delta HOMA_{S-T}$ and ΔISE_{S-T} .^[93] Additionally, the vertical excitation energies to S_1 were found to vary with the degree of S_0 aromaticity.

An elegant spectroscopic evidence for a switch in aromatic and antiaromatic character (and vice versa) when going from S_0 to T_1 was provided by Kim, Osuka and co-workers through the ground and excited-state absorption spectra of a pair of bis-rhodium hexaphyrins; one with 26 π -electrons which is

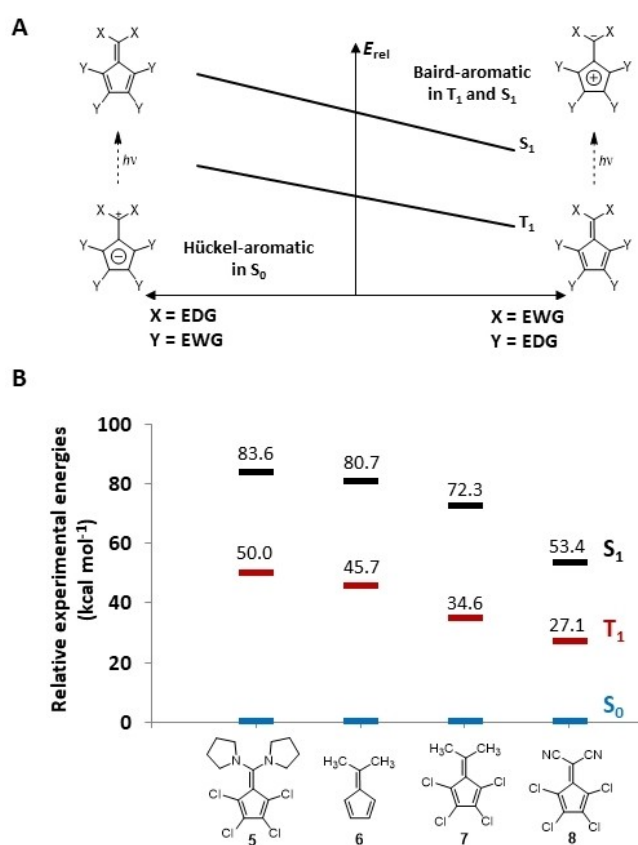


Figure 3. A) Schematic energy diagrams that display the tuning of S_1 and T_1 state excitation energies of pentafulvene through substitution: substituents X and Y impact on the S_1 and T_1 state energies of pentafulvenes, either enhancing the S_0 -state Hückel aromaticity (X = electron-donating group, EDG, or Y = electron-withdrawing group, EWG) or the S_1/T_1 -state Baird aromaticity (X = EWG or Y = EDG). B) Experimentally determined S_1 - and T_1 -state excitation energies [kcal mol⁻¹] of four differently substituted pentafulvenes.^[91–93]

aromatic in S_0 and one with 28 π -electrons which is antiaromatic.^[94] In the S_0 state, the aromatic hexaphyrin has a sharp absorption spectrum while the antiaromatic one displayed a broad and structureless spectrum. When going to the T_1 state, the spectral features switched character, and this, together with computationally determined aromaticity indices, provided evidence for Baird's rule operating in a pair of closely related compounds having opposite aromatic/antiaromatic characters. Similar observations were made for a pair of 1,3-phenylene strapped [26]- and [28]hexaphyrins for the singlet excited state.^[95] Due to this light-induced switch in the aromatic/antiaromatic characters, the hexaphyrin pairs can be labeled as a light-switched yin-yang pairs.^[96] Later on, support for the aromaticity and antiaromaticity reversal has also been obtained by time-resolved vibrational spectroscopy.^[14,17,97]

Although the cyclopentadienyl cation and its pentachloro congener have triplet ground states according to EPR spectroscopy,^[70,98] which also applies to hexachlorobenzene dication,^[99] it was only recently that such a species could be isolated and studied by crystallography. Long and co-workers used two gadolinium trications in an inverse sandwich structure to exercise direct magnetic exchange couplings and force the central benzene dianionic moiety to adopt a Baird-aromatic triplet ground state.^[100]

Taken together, it is clear that Baird aromaticity and antiaromaticity of $\pi\pi^*$ excited states as well as triplet ground states have potentials for numerous areas. To provide a basis for applications within photoinduced reactivity we next discuss how ESA gain and ESAA relief impact on the shapes of excited-state potential energy surfaces.

4. Effects of ES(A)A on the Excited-State Potential Energy Surface

Photoinduced reversal of (anti-)aromaticity from the S_0 state to the lowest $\pi\pi^*$ excited states brings changes to various physicochemical properties of $[4n]$ - and $[4n+2]$ annulenes. For a comprehensive treatise of these impacts, we refer to our previous reviews,^[13,14] yet, in this section we describe how the ES(A)A character influences properties linked to reactivity, particularly the shapes of the excited-state potential energy surfaces (PESs). Hence, the aromatic stabilization energies (ASEs) are crucial as they reflect the gain (loss) in energy upon attainment of aromaticity (antiaromaticity) when compared to a suitable nonaromatic reference. These energies were first assessed for $[4n]$ annulenes in their triplet states by Gogonea, Schleyer and Schreiner,^[69] and later by Zhu, An and Schleyer for a broader class of species including both $[4n]$ - and $[4n+2]$ annulenes as well as 4π -electron heteroannulenes.^[54,55]

As noted above, a particularly attractive ASE is the isomerization stabilization energy (ISE, Figure 4). The ISEs in the T_1 states are generally found to be, respectively, positive for $[4n+2]$ annulenes and negative for $[4n]$ annulenes, opposite to those in the S_0 states. The ISE_I of benzene in S_0 is -33.2 kcal mol⁻¹, revealed through a stabilization of toluene (10) relative to its

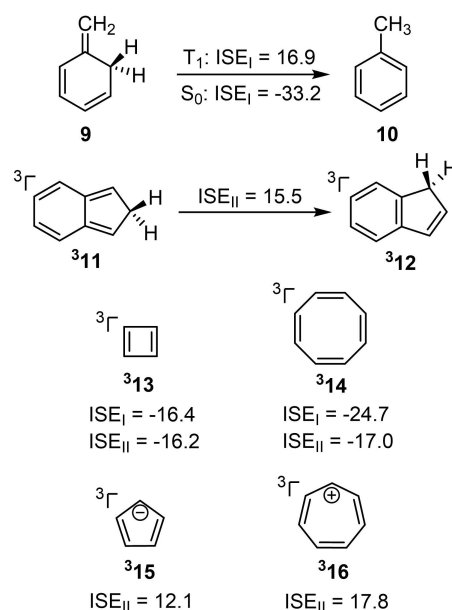


Figure 4. Isomerization stabilization energies (ISEs [kcal mol⁻¹]) of some representative $[4n]$ - and $[4n+2]$ annulenes. The ISEs for benzene are given both for S_0 and T_1 ; for the other compounds, the ISEs are only given for the T_1 states, although they are calculated in two different ways.^[54,55]

nonaromatic isomer 9.^[9] In contrast, in T_1 the ISE changes sign to 16.9 kcal mol⁻¹, revealing a destabilization of 10 compared to 9 (Figure 4). In addition to exploring ISE's of various $[4n]$ - and $[4n+2]$ annulenes in the S_0 and T_1 states, An and Zhu also calculated the energy differences between the cyclic compound and their directly cleaved acyclic reference compounds in homodesmotic reactions. These energies showed good correlations to the earlier computed ISEs.^[101]

Excited-state aromatic stabilization and antiaromatic destabilization are also reflected in the first hydrogenation energies of, respectively, $[4n]$ - and $[4n+2]$ annulenes, as revealed by Papadakis et al. (Figure 5A).^[102] Computationally, they showed that the first hydrogenation steps of $[4n+2]$ annulenes were exergonic in the T_1 states, in contrast to the S_0 states where they are endergonic. The opposite applies for $[4n]$ annulenes. Noteworthy, for each state there is a zigzag relationship between the energies of the first hydrogenation step and the π -electron counts (Figure 5B), and importantly, the zigzag relationship is opposite for the two states which provides support for the switch in aromatic and antiaromatic character when going from S_0 to T_1 . Thus, the high hydrogenation reactivities of arenes in their T_1 states observed in the experiments stem from a drive to alleviate the antiaromatic destabilization, while the decreased reactivity of $[4n]$ annulenes reflects the loss of aromatic stabilization through the hydrogenation reaction.

The drive to alleviate ESAA and its effect on excited-state potential energy surfaces is demonstrated through the discovery of a small red emitter based on a single benzene fluorophore moiety.^[103] Despite that 1,10-(2,5-diamino-1,4-phenylene)bis(ethan-1-one) (*p*-DAPA, 17) lacks extended π -

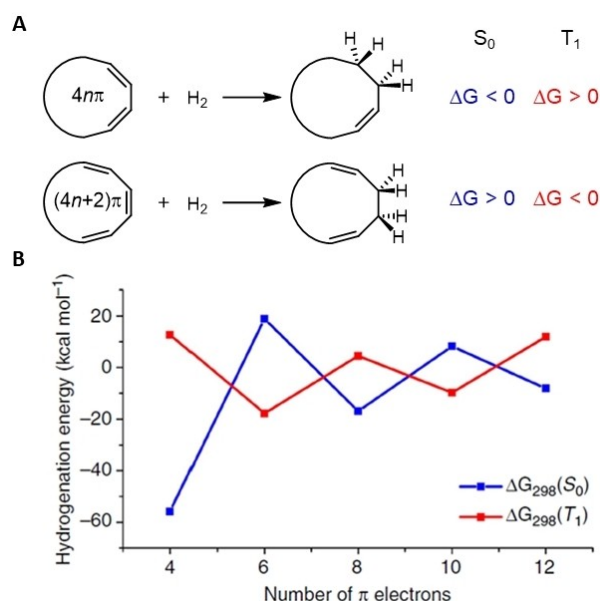


Figure 5. A) Hypothetical schemes of the first hydrogenation and energy sign reversal of $[4n]$ - and $[4n+2]$ annulenes from the S_0 to the T_1 state. B) Zigzag relationship between π -electron counts and the first hydrogenation energies, calculated at the (U)B3LYP/6-311+G(d,p) level for annulenes (neutral, cationic and anionic) with 4, 6, 8, 10 and 12 π -electrons. Each data point is an average of a number of annulenes and annulenyl cations/anions. Reproduced from ref. [102], which is an open access article distributed under the terms of the Creative Commons CC BY license.

conjugation or intramolecular charge transfer character of its excited state, it was found to emit red light ($\lambda_{em} = 618$ nm). The unusually small energetic difference between the S_1 and S_0 potential energy surfaces in the S_1 relaxed geometry was attributed to ESAA alleviation assisted by intramolecular hydrogen bonds. For example, as demonstrated by NICS(1)_{zz} values (Figure 6A, B), *p*-DAPA is aromatic in S_0 but becomes antiaromatic upon vertical excitation to its S_1 state. Yet, the S_1 state relieves most of this antiaromaticity through hydrogen bond length redistribution between the amino and the adjacent carbonyl group, and the emission occurs from this relaxed minimum. Support of this interpretation is also provided by HOMA (Figure 6C, D, based on S_0 HOMA parameters).

Benzannulated $4n\pi$ -electron molecules can also show emissive properties (Figure 7A),^[87] yet, here the structural change is driven by gain of ESA. $[4n]$ Annulenes and various benzannulated derivatives are often puckered in S_0 , and to gain aromatic stabilization in their lowest excited states they planarize. Various computed aromaticity indices (MCI, NICS, and HOMA) have verified that the planar structures are aromatic in both their S_1 and T_1 states.^[89] For instance, a NICS-XY scan of dibenz[*b,f*]oxepin (**4**) revealed a clear Baird-aromatic character for the planar T_1 state structure (NICS = -15.2 ppm at the center of the oxepin ring), and the compound exhibits higher HOMA values for the 16π -electron perimeter in S_1 and T_1 (0.770 and 0.675, respectively) than in S_0 (0.530).

Although intricate, the excited-state aromatic stabilization can be quantified experimentally as revealed by Itoh, Aida and

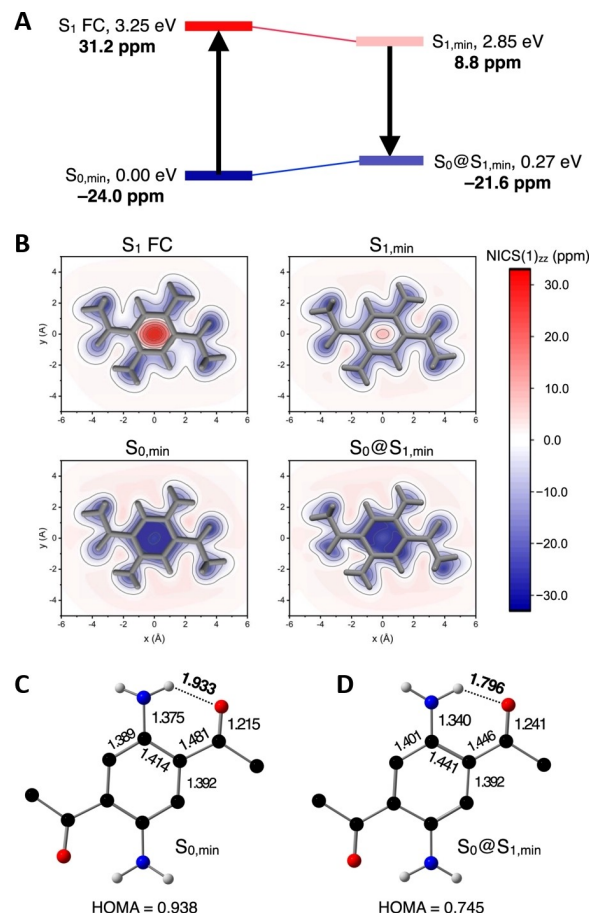


Figure 6. Relief of ESAA assisted by intramolecular hydrogen bonds. A) Schematic energy diagram with calculated NICS(1)_{zz} values (in bold) at the optimized geometries of *p*-DAPA. FC: Franck–Condon. B) Calculated NICS(1)_{zz} grids parallel to the molecular plane of *p*-DAPA. Bond lengths [Å] and HOMA value of *p*-DAPA at the C) $S_{0,min}$ and D) $S_0@S_{1,min}$ geometries. Reproduced from ref. [103], which is an open access article distributed under the terms of the Creative Commons CC BY license.

co-workers for a chiral cyclooctatetrathiophene with an 8π -electron cyclooctatetraene (COT) core (**18**, Figure 7B).^[104] In its S_0 state, this molecule has a tub-shaped conformation due to steric strain between the four thiophene rings in addition to the intrinsic angle strain in the COT ring. When **18** ring-inverts from one enantiomer to the other it needs to proceed via a quasi-planar TS, and thus, it needs to overcome both the steric and angle strains leading to an inversion barrier which is significantly higher in the S_0 state (25.4 kcal mol⁻¹) than for the parent COT molecule (~12 kcal mol⁻¹).^[105,106] However, it was found through a combination of the CD spectral decay profiles and computations that aromaticity is gained in the lowest $\pi\pi^*$ states when the central COT ring of **18** becomes planar, leading to lowering of the activation barrier for inversion by 21–22 kcal mol⁻¹ relative to the barrier in S_0 ($\Delta\Delta H^\ddagger_{inv}$, Figure 7B). This value provides an experimentally determined excited-state ASE value.^[104] Noteworthy, the lowering is the same in the T_1 and S_1 states, indicating that the S_1 state of **18** is aromatic to a similar extent as the T_1 state, a finding supported by computational results.

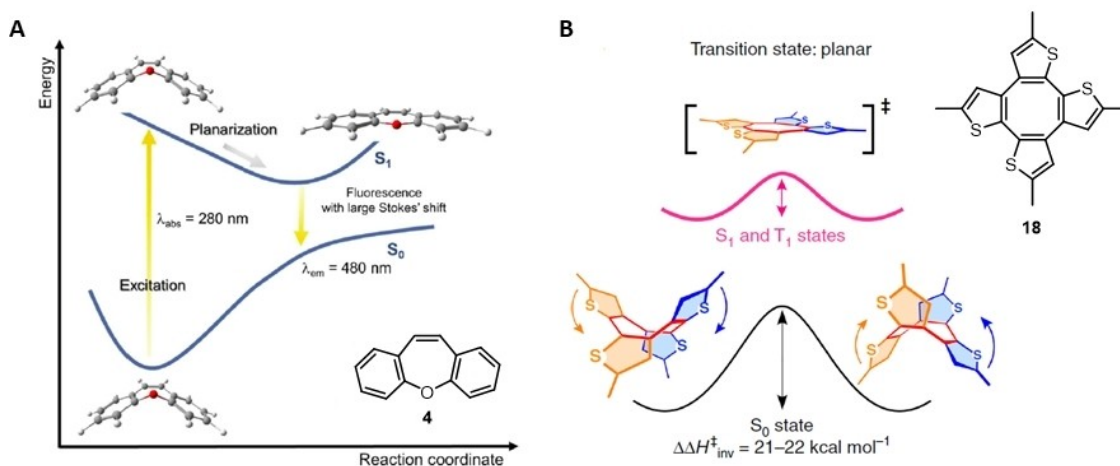


Figure 7. A) Photoexcitation of dibenz[b,f]oxepin from the S₀ to the S₁ state and their potential energy surfaces (PESs). Reproduced with permission from ref. [89]. Copyright: 2019, Wiley-VCH Verlag GmbH & Co. KGaA. B) Ring inversion of thiophene-fused chiral COT where $\Delta\Delta H_{\text{inv}}^{\ddagger} = \Delta H_{\text{inv}}^{\ddagger}(S_0) - \Delta H_{\text{inv}}^{\ddagger}(T_1)$. Reproduced from ref. [104], which is an open access article distributed under the terms of the Creative Commons CC BY license.

Thus, excited-state aromaticity is a stabilizing factor according to both computational and experimental observations, and it should have an impact on photoreactivity. Indeed, when investigating the singlet excited-state PESs linking various excited-state C₈H₈ isomers, transition states and conical intersections, Garavelli et al. conclude that “a planar D_{8h}-symmetric minimum [of COT] represents the collecting point on S₁” and they considered it as “stabilized by a kind of aromatic effect”.^[107] This interpretation is supported by the joint experimental and computational study by Ayub et al. using the cyclopropyl (cPr) group as an indicator to differentiate the triplet state aromaticity from the antiaromaticity or nonaromaticity of [4n + 2](hetero)annulenes.^[108] Normally, the cPr group ring-opens when attached to singlet and triplet diradicals,^[109–112] yet, when attached to a 4nπ-electron annulene which is T₁ (and S₁) state aromatic this process should be unfavorable as it would ruin the excited-state aromaticity (Figure 8A). Indeed, in experiments it was found that the cPr group, when attached to T₁ antiaromatic benzene or naphthalene (³19 and ³22), undergoes facile homolytic ring-opening upon irradiation in methanol at λ = 254 nm with a regain of aromaticity in the annulenic moiety and subsequent solvent addition followed by polymerization (19) or decomposition (22). In contrast, when attached to an S₁ and T₁ aromatic COT (25), the cPr group becomes inert under the same photochemical conditions, since the ring-opening would cause a loss of COT aromaticity (Figure 8B). As benzene has lower intersystem crossing quantum yield (Φ_{ISC} = 0.25)^[113] than naphthalene (Φ_{ISC} = 0.75),^[114] it is likely that the photo-reaction of 19 occurs either only from triplet, or from both the S₁ and T₁ states, while the photodegradation of 22 should occur solely from the T₁ state. On the contrary, the Φ_{ISC} of COT is rather low^[115] so that 25 will remain in the S₁ state, unless triplet sensitizers are used.

However, the activation energy for cPr ring-opening may primarily depend on the spin density at the C atom to which the cPr group is attached, and that it is higher in ³25 than in ³19

simply because the spin density is evenly distributed over the ring while it is localized to certain C atoms in the latter. Indeed, for a set of nonaromatic reference compounds in their T₁ states there is a strong correlation (R² = 0.931, Figure 8C) between the site-specific spin density and the activation barrier for cPr ring opening. Yet, the activation barriers for cPr opening in cPr-substituted annulenes depend additionally on the π-electron count of the annulene. More specifically, the cPr-substituted 4nπ-electron (hetero)annulenes have higher activation barriers by 1.6–6.0 kcal mol^{−1} than a hypothetical nonaromatic analogue with the same spin-density at the C atom to which the cPr group is attached, while for the cPr-substituted (4n + 2)π-electron (hetero)annulenes the activation barriers are lower by 1.7–7.7 kcal mol^{−1} than had the (hetero)annulenic rings been nonaromatic. This reveals (de)stabilizing effects of Baird (anti-)aromaticity in the T₁ state which turns to nonaromatic character upon cPr-ring opening. An analogous trend was found computationally for the S₁ states.^[108] Similarly, the silacyclobutene moiety was also identified as a good T₁ aromaticity indicator.^[116] For example, silacyclobutene-fused [4n + 2]annulenes displayed increased photoreactivity,^[117] but when this moiety is fused to [4n]annulenes, its ring-opening is endergonic as this reaction would break the Baird aromaticity.^[116]

As the cPr group is a reoccurring structural unit in novel drugs and drug candidates,^[118] there could be reasons to pay attention to potentially lower photostability of drugs and drug candidates containing cPr substituent on a (hetero)annulene moiety. Other small and strained groups (e.g., the bicyclo[1.1.1]pentyl group) are found as saturated phenyl bioisosteres in novel drugs.^[119] Also for these there could be reasons for caution with regard to possible photodegradation when attached to cyclic moieties with (4n + 2)π-electrons.

Related to the findings on cPr-substituted annulenes, the T₁ PES's of annulenic substituted olefins also vary in an interesting way (Figure 9).^[120–123] Upon excitation of styrene (26) from S₀ to

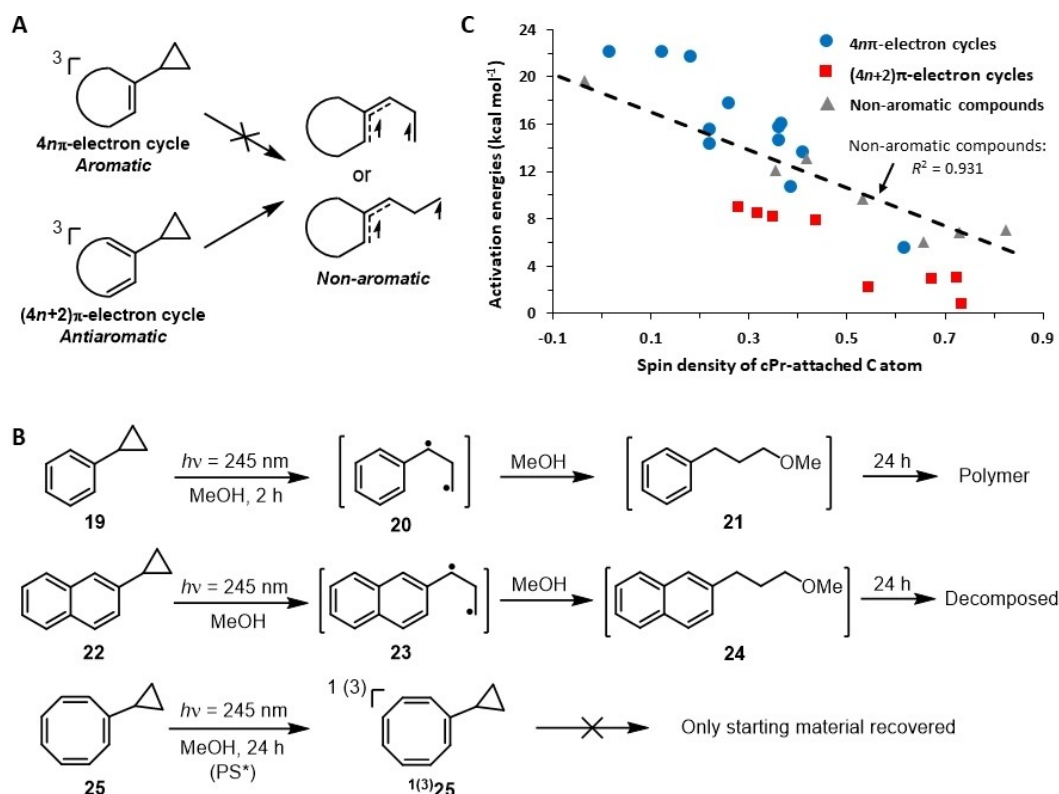


Figure 8. A) Ring-opening of cPr-substituted $4n\pi$ - and $(4n+2)\pi$ -electron cycles in the T_1 state. B) Experimental cPr ring-opening of cPr-benzene, cPr-naphthalene and cPr-COT, PS*: photosensitizer. C) Activation free energies of $4n\pi$ - and $(4n+2)\pi$ -electron cycles against the calculated spin density (delocalization level) at the C atom to which cPr group is attached in the T_1 state. Figure based on results from ref. [108].

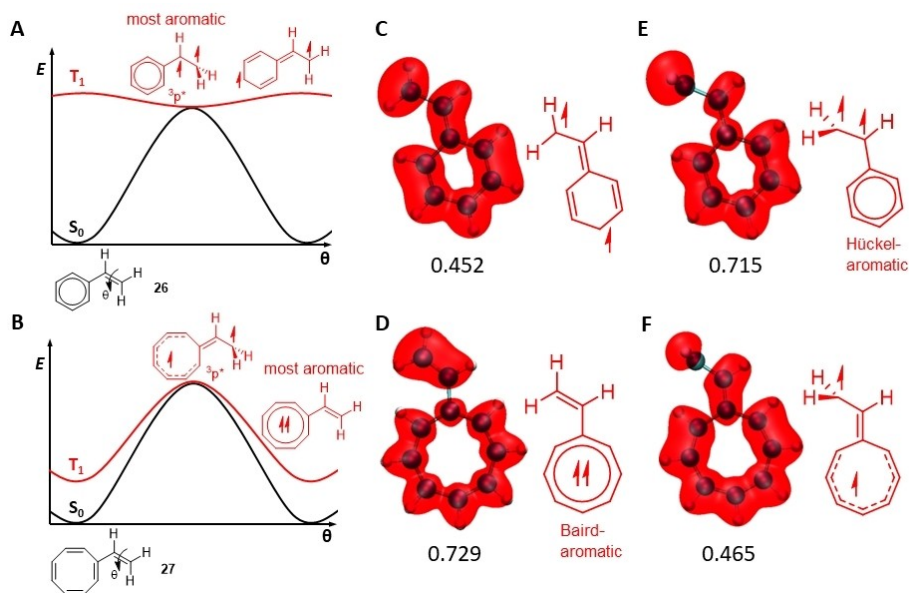


Figure 9. T_1 -state Z/E isomerization of A) styrene- and B) COT-substituted olefins with the ring-closure bifurcation values of the basins of the π -contribution to the electron localization function (RCBV(ELF _{π})) as the ring aromaticity indicator (C and E for vinylstyrene and D and F for vinylCOT). RCBV(ELF _{π}) values above 0.65 reveal aromaticity. Figure based on results from ref. [122].

T_1 , the phenyl group becomes antiaromatic (Figure 9A and C). However, as a means to alleviate this T_1 antiaromaticity the

olefin bond twists to 90° so that at the T_1 state minimum **26** is described as a 1,2-biradical composed of a Hückel-aromatic

benzyl radical part and a methyl radical part (Figure 9A). This partial regain of Hückel aromaticity is viewed through the π -contribution of the electron localization function (ELF_π), more explicitly in the ring-closure bifurcation values in ($\text{RCBV}(\text{ELF}_\pi)$).^[48] These values should be above 0.65 for aromaticity.^[124] Clearly, the twisted minimum structure ($^3\text{p}^*$) of **326** is the most aromatic.^[122] In contrast, $[4n]$ annulenyl substituted olefins are aromatic in T_1 and tend to keep the biradical character within the annulenyl ring (Figure 9B). As a consequence, the olefinic C=C bond of vinylCOT (**27**) remains a rigid double bond in T_1 and twisting about this bond leads to loss of T_1 state Baird aromaticity of the COT ring (Figure 9D and 9F). This explains the very low quantum yields observed for the *Z/E*-photoisomerization of 1,5-bis(styryl)-cyclooctatetraene when run under sensitized conditions.^[125]

Substituted olefins **26** and **27** represent the two extreme cases. Quantum chemical computations reveal that by choice of the olefin substituents as different five-membered ring 6π - and 4π -electron heteroannulenes, together with the cyclopentadienyl anion and cation, it is possible to tune the shape of the T_1 PES between the two extremes.^[123] The ESA and ESAA effect of the annulenyl group as a substituent on the olefin also attenuates as one goes to larger ring systems.^[121]

Thus, the vinyl group of **26** functions as a substituent that assists in alleviating the T_1 state antiaromaticity by twisting, similar to what the cPr group does by ring-opening. In general, substituents can have notable influence on antiaromaticity reduction in the lowest excited states, as revealed by Baranac-Stojanović for substituted benzenes in their T_1 states.^[126] The calculations revealed, for example, that benzenes with σ - or π -electron-donating substituents are less antiaromatic than simple benzene in the T_1 state. Carbonyl and nitro substituents, at which the triplet diradical character can localize, lead to benzene rings with significant aromatic character in the T_1 state,^[126] which, however, should be Hückel-type aromaticity. Thus, the substituent on a benzene ring impacts also on its antiaromaticity (or aromaticity) in the T_1 state, affecting the photoreactivity of the compound in question. For the 8π -electron COT ring, it has been found that amido substituents have very small effects on the T_1 aromaticity.^[127] Clearly, the triplet excitation is confined to the Baird-aromatic COT ring whereby substituents have only modest effects. Thus, the effect of a certain substituent depends on which type of ring it sits (a $4n\pi$ - or $(4n+2)\pi$ -electron ring), as shown above for the cPr group.

Generalizing these findings on the connection between the shapes of the T_1 and S_1 PES's and ESAA relief or ESA gain, one can draw the qualitative schemes of Figures 8A and B, respectively. For an excited $[4n+2]$ (hetero)annulene derivative, the extent of antiaromatic character in the idealized case attenuates gradually as the molecule moves along on the S_1 and T_1 PES until it reaches a conical intersection with the S_0 state (Figure 10A), or alternatively, it reaches an excited-state minimum with a weak antiaromatic or nonaromatic character from where it relaxes radiatively or non-radiatively. In contrast, a $[4n]$ (hetero)annulene in its lowest $\pi\pi^*$ vertically excited state is only weakly aromatic or nonaromatic. By the structural

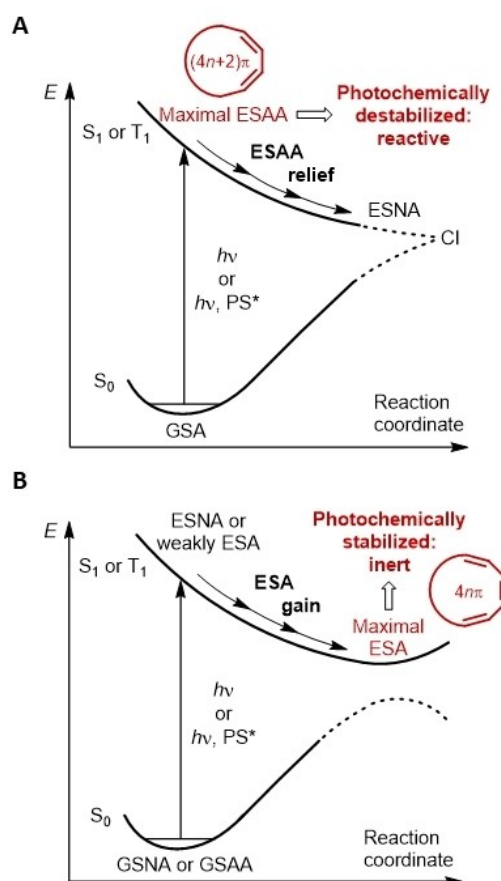


Figure 10. Schematic drawings of idealized PES shapes in the S_1 and T_1 states for A) ESAA relief and B) ESA gain. GSA: ground-state aromaticity, GSAA: ground-state antiaromaticity, ESNA: excited-state nonaromaticity, CI: conical intersection.

relaxation, leading to a more planar and bond length equalized structure (Figure 10B), it will gradually gain ESA until it reaches the highly symmetric minimum on the S_1 or T_1 state PES with maximal excited-state Baird-aromatic character.

5. ESA and (Lack of) Photoreactivity

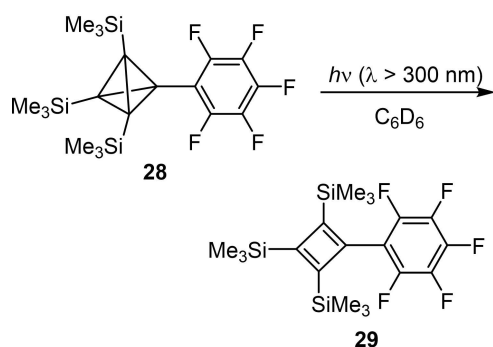
So far, there have only been a few explicit studies on the relationship between ESA and photoreactivity of $[4n]$ annulenes or of photoreactions leading to such species. As mentioned above, Garavelli et al. described the D_{8h} -symmetric minimum of COT as “a collecting point on S_1 ” stabilized by “a kind of aromatic effect”.^[107] This gain of ESA should promote photochemical formation of various COT and 8π -electron heteroannulene derivatives (Figure 10B), and in a previous review we described a series of such photoreactions leading to interesting 7- and 8-membered rings with further synthetic potentials.^[13] We also listed thirteen pathways for photochemical formation of the parent cyclobutadiene (CBD) at cryogenic temperatures starting from various precursors. Yet, until today there is no combined experimental-computational study that shows on the gain of

ESA along the reaction coordinates of these reactions. Indeed, the decay to the S_0 state may occur through a conical intersection before the reacting system has reached the highly symmetric Baird-aromatic structure of a $4n\pi$ -electron species in its lowest excited states.

5.1. Monocyclic $4n\pi$ -electron species

With regard to a CBD derivative formed photochemically at ambient temperature the tris(trimethylsilyl)pentafluorophenyl-cyclobutadiene (**29**) is formed from tris(trimethylsilyl)-pentafluorophenyl-tetrahedrane (**28**) upon irradiation with $\lambda > 300$ nm (Scheme 2).^[128] This reaction should occur in the S_1 state, and it can be an effect of both ESAA within the phenyl group, which triggers the opening of the tetrahedrane moiety, and gain in ESA when the CBD ring is formed. In this context, it is noteworthy that the S_1 state of the parent CBD in the D_{4h} symmetric structure has been found to be significantly influenced by aromaticity as it has a NICS value of -16.5 ppm at CASSCF level,^[72] and the T_1 state has a NICS value which is very similar (-16.4 ppm). In a recent investigation using temperature-dependent EPR experiments, it was observed that the T_1 state of *tetrakis*(trimethylsilyl)cyclobutadiene (**30**) can be populated thermally and that it is situated 13.9 kcal mol $^{-1}$ above the S_0 state.^[129] The D parameter from the recorded EPR spectrum of the T_1 state revealed a square geometry, and the very minor computed distribution of triplet state spin density onto the silyl substituents (SiH_3 or SiMe_3) is consistent with T_1 state Baird aromaticity. Interestingly, this CBD derivative is thermally stable and decomposes to bis(trimethylsilyl)acetylene first at 250 °C.^[130] Still, the potential Baird aromaticity of **30** in its T_1 state was not determined explicitly.^[129]

As $[4n+2]$ annulenes are inert in their S_0 states, one can expect $[4n]$ annulenes to be inert when excited to their S_1 and T_1 states. Indeed, Paquette and co-workers observed that both 1,2-dimethylCOT (**31** and **32**) and 1,4-dimethylCOT (**33** and **34**) when irradiated under sensitized conditions were stable for 100 h (Figure 11A), contrasting their ready thermal rearrangements.^[131] Furthermore, under conditions where benzene readily adds triethylsilane under irradiation, COT (**13**)



Scheme 2. Photochemical formation of tris(trimethylsilyl)pentafluorophenyl-cyclobutadiene from tris(trimethylsilyl)pentafluorophenyl-tetrahedrane.^[130]

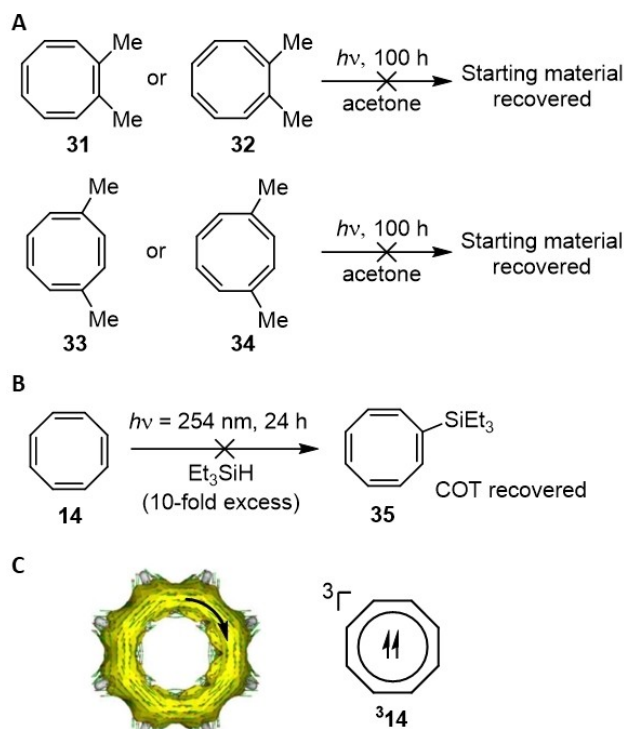


Figure 11. A) Photostability of 1,2-dimethylCOT and 1,4-dimethylCOT.^[131] B) Attempted photochemical addition of triethylsilane to COT. C) ACID plot of T_1 -state COT revealing an induced diatropic ring-current.^[102]

remained completely inert (Figure 11B), consistent with its Baird-aromatic stabilization.^[102]

The photostability of COT can be used in applications because when covalently linked to a chromophore it can enhance the photostability of the latter as demonstrated for fluorophores for bioimaging,^[127] zinc porphyrins,^[132] and organic laser diode materials.^[133] Two aspects are important for this function, and both relate to the T_1 state aromaticity of COT (**14**). First, intramolecular triplet energy transfer to the attached COT moieties is efficient, whereafter its T_1 state aromatic minimum decays to the S_0 state. This provides, for example, a COT-linked fluorophore with a self-healing feature.^[134] With this, one avoids build-up of the fluorophores' T_1 states which are phototoxic by themselves, induce photoreactions, such as H-atom abstractions, and lead to the formation of reactive oxygen species (ROS). A second important aspect of $^3\mathbf{14}$ is its low propensity to form singlet oxygen through triplet-triplet annihilation as the reaction leading from $^3\mathbf{14}$ and $^3\text{O}_2$ to **14** in its S_0 state and singlet oxygen is endergonic for COT derivatives while the analogous processes are exergonic for common Hückel-aromatic triplet energy quenchers such as anthracene.^[127] Both these aspects are related to the T_1 state Baird-aromatic character of COT.

A number of photochemical approaches to $[4n]$ annulenes were shown in our previous review from 2014.^[13] An early gas phase study, relevant to the growing area of astrochemistry, reveals the formation of four tetracyanoCOT isomers (**37–41**) as major products and two tricyanobenzenes (**42** and **43**) as minor

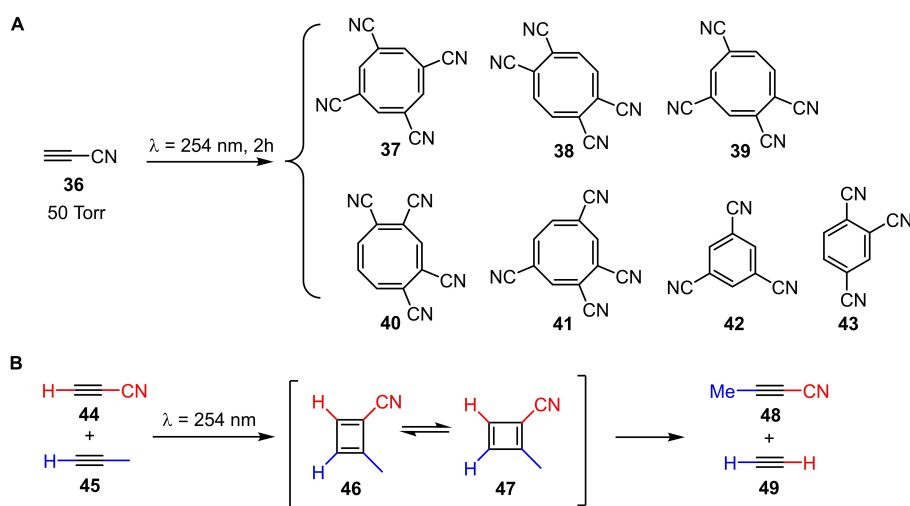
products when cyanoacetylene was irradiated with 254 nm light at 50 Torr (Scheme 3A).^[135] More recent gas-phase irradiation experiments (also at $\lambda = 254$ nm) on mixtures of cyanoacetylene and propyne revealed the formation of methylcyanoacetylene and acetylene, a process that proceeds by excitation of cyanoacetylene and the likely formation of a transient cyanomethyl substituted cyclobutadiene **46** and its bond-shift isomer **47** (Scheme 3B).^[136]

5.2. Polycyclic molecules with 4 π -electron cores

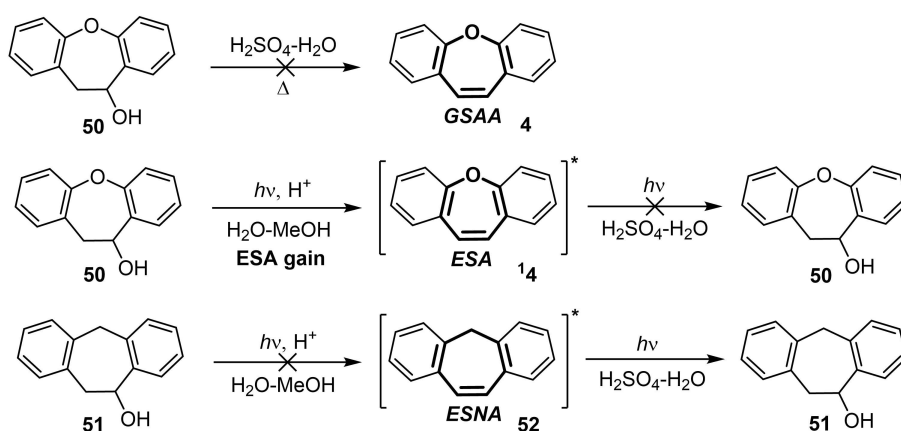
Dibenzo[*b,f*]oxepin (**4**) is an oxepin derivative that exhibits a similar attenuated photoreactivity as that of COT.^[87] When photoexcited this molecule shows a notably different photoreactivity compared to its thermal reactivity and also compared to the photoreactivity of its analogue suberene **52** which has a nonaromatic middle ring. Formation of dibenz[*b,f*]oxepin by dehydration of **50** is thermally difficult but facile under photo-

chemical conditions (Scheme 4). In contrast, attempts to afford suberene through alcohol **51** dehydration under the same conditions failed. Also, photoreduction and photoaddition of the alkenyl group in dibenz[*b,f*]oxepin are much less efficient than in suberene. This photoreactivity difference was also found between dibenz[*b,f*]oxepin and dihydrodibenz[*b,f*]oxepin since photolysis of the latter afforded a spiro adduct (possibly via a radical pathway) while the former was inert (Scheme 4).

The excited-state aromatic stabilization of dibenz[*b,f*]oxepin (19.6 kcal mol⁻¹) decreases with flattened *S*₁ state PES if further π -expansion is introduced into the structure (Figure 12).^[137] For example, the COT-fused anthracene dimer undergoes conformational planarization in the *S*₁ state due to the contribution of the Baird-aromatic COT ring. However, if the two π -conjugated acene segments are exchanged to tetracene or pentacene moieties, then the contribution of acene segments to the *S*₁ state outperforms the contribution of the COT ring.^[138] In such cases the molecule does not planarize in the *S*₁ state. Instead, one can observe a singlet exciton fission process as the



Scheme 3. Photochemical formation of A) tetracyanocyclooctatetraenes as major products and tricyanobenzenes as minor products in irradiation experiments of cyanoacetylene. B) Photochemical formation of transient 1-cyano-2-methylcyclobutadiene as the two bond-shift isomers and its subsequent retro-cycloaddition reaction.



Scheme 4. Synthesis and photoreactivity of dibenz[*b,f*]oxepin and suberene.

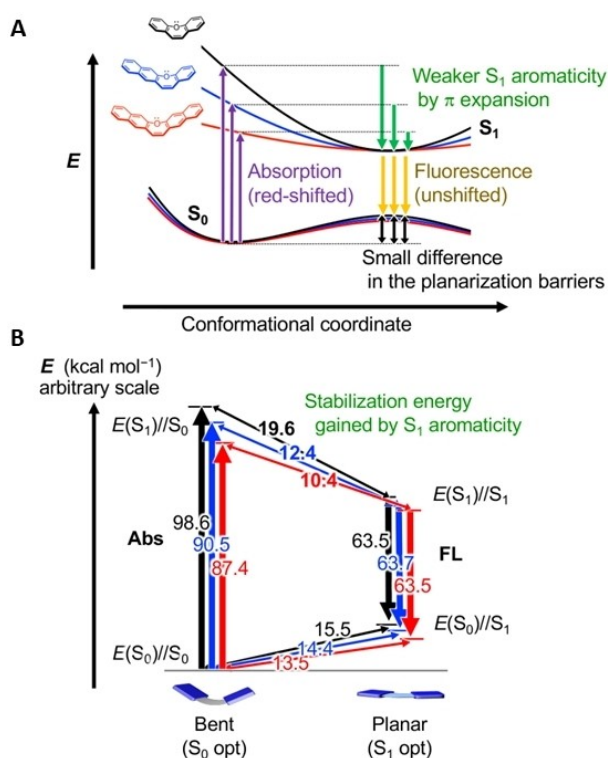


Figure 12. A) Tuning S₁ aromaticity and PES's with π expansion of oxepin. B) Relative energy levels of π-expanded oxepins in the S₀ and S₁ states. Reproduced with permission from ref. [137]. Copyright: 2020, American Chemical Society.

molecule in these cases is best described as two tetracene or pentacene moieties linked by two ethylene tethers.

Also other dibenzannulated 8π-electron heteropines have been investigated. Chen et al. observed large Stokes shifts for a series of (N-substituted)dibenz[*b,f*]azepins that are attributed to the ESA-driven planarization along the S₁ PES with a negligible barrier.^[139] For *N*-phenyl dibenz[*b,f*]azepins, a phenyl ring rotation is involved in the planarization and induces a barrier, which can be lowered by decreasing the electron-donating ability of the *para*-substituent on the phenyl ring. In this context, it is noteworthy that Padberg et al. observed nearly the same Stokes shifts for isomeric dithienophosphepines and their corresponding oxides (non-(anti-)aromatic analogues), which

indicates that large Stokes shifts are not always related to the S₁ planarization and the attainment of ESA character.^[140]

Returning to the seminal work by Wan on photosolvolysis of fluorenol (see above),^[83] this molecule has been identified as a scaffold undergoing efficient photoheterolysis producing excited 4π-aromatic fluorenyl cation. The ESA gain facilitates efficient cleavage of even poor leaving groups, such as hydroxide anion,^[83] carboxylates^[141] or tertiary amines.^[142] Recently, Heckel and co-workers developed a series of 9-fluorenol-based photoremovable protecting groups **53** (photocages) based on this photoreactivity.^[143,144] Dialkyl and diarylamino substitution in positions 2 and 7 (Figure 13A) led to red-shifted absorption ($\lambda_{\text{abs}} \leq 369$ nm) and high uncaging quantum yields ($\Phi_r \leq 0.42$). The second generation of ESA-driven photocages was rationally designed by computation of excitation energies of various heterocycle-fused cyclopentadienyl carbocations **54**.^[143] The small vertical excitation energy of the cationic intermediates with large antiaromatic S₀ state character and large ESA character was hypothesized as a measure of a productive photoheterolysis. *Para*-thio-cyclopentadithiophene derivatives **55** (Figure 13B) were identified as molecules with large antiaromatic character in the S₀ (NICS(0, outer rings) = 22.7 ppm, NICS(0, inner ring) = 96.8 ppm; note that NICS(0) is known to exaggerate the σ-contributions and artificially increases the NICS value)^[32] and lowest vertical excitation energy of the corresponding cyclopentadienyl carbocation (0.73 eV vs. 1.61 eV for fluorenyl carbocation). These compounds were found to be efficient UV-to-blue light-driven photocages with moderate uncaging quantum yields ($\Phi_r = 0.03$ –0.28) and satisfactory uncaging cross sections ($\epsilon\Phi_{r,405\text{ nm}} = 600$ –900 M⁻¹ cm⁻¹).

5.3. Synopsis

To summarize, the photoreactivity leading to 4nπ-electron cycles as well as the photostability of such cycles once formed support the validity of the general features of the excited-state PES described in Figure 10B. Until today, the reaction types that have been used for formation of 4nπ-electron cycles (Figure 14) involve various photorearrangements, photoadditions, photoeliminations (further examples in ref. [12]), and excited-state protonations of (4n + 2)π-electron species (discussed in the next section) which lead to excited-state homoaromatic 4n-electron

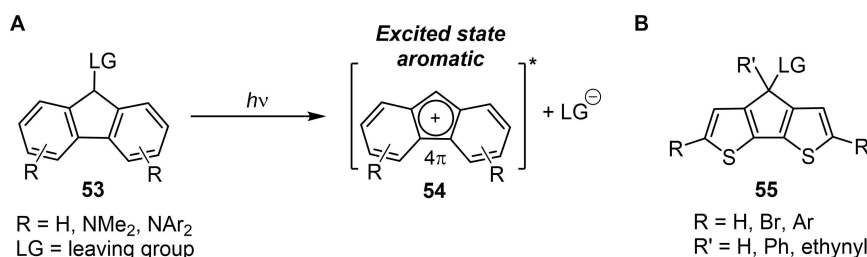


Figure 13. A) A 9-fluorenyl-based photoremovable protecting group forming excited-state aromatic carbocation. B) Cyclopentadithiophene photoactivatable derivatives.

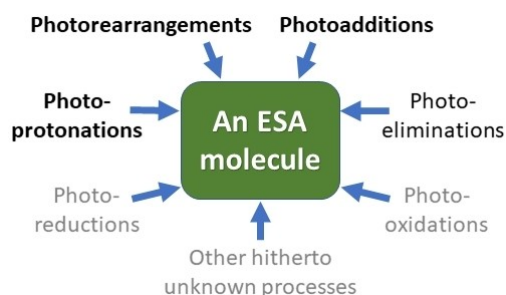


Figure 14. The various processes by which a molecule can be formed through gain of ESA. Processes in bold are discussed herein, those in normal print in ref. [12]. Photochemical processes of the reaction types in gray have not yet been reported.

species. So far, there are no reports on photooxidations or photoreductions leading to cyclic $4n\pi$ -electron compounds, possibly as these species would rapidly recapture electrons or holes expelled in such processes. Yet, this opens for future research. In this context, one can note that the T_1 state ISE values for several small and medium-sized macrocycles with aromatic 6π -electron monocycle units (e.g., $[n]$ cycloparaphenylenes, $[n]$ CPPs) are negative due to formation of globally Baird-aromatic cycles with $n \times 4 \pi$ -electrons.^[26] Thus, there may exist hitherto unknown photorearrangement paths to such macrocycles. Indeed, the COT dimer is known to ring-open photochemically to [16]annulene, although in just 13% yield.^[145]

Taken together, the rather limited number of reaction types suggests that there is (much) more to be explored in the area of photochemical formation of $4n\pi$ -electron cycles. In the next section, we analyze photoinitiated processes that lead to ESAA alleviation.

6. Relief of ESAA

As described in Figure 10A, an S_0 aromatic molecule in its lowest $\pi\pi^*$ state should strive to alleviate its antiaromatic character. As will be seen next, this ESAA alleviation can proceed by a number of different processes. It can be by unimolecular processes enabled by puckering allowing the molecule to reach a conical intersection, or by electron transfer from one moiety of the molecule to another. The ESAA alleviation can also proceed through a bimolecular reaction. The photoreactions are found in a variety of applications; from drug photodegradation in pharmaceutical chemistry to molecular design of optical switches for optoelectronics.

6.1. Photorearrangements of 6π -electron cycles

Benzene is the archetype of an aromatic molecule in S_0 ($\text{NICS}(1)_{zz} = -27.4$ ppm), and its isomerization upon photoexcitation exemplifies the enhanced reactivity of $[4n+2]$ annulenes in their excited states.^[68] This photoreactivity was recently linked

to ESAA relief by Slanina et al. (Figure 15),^[146] as benzene at its S_1 minimum is markedly antiaromatic ($\text{NICS}(1)_{zz} = 80.9$ ppm). This excited-state antiaromatic benzene molecule relieves its destabilization through a rearrangement resulting in the formation of either of two nonaromatic isomers, pentafulvene (**58**) and benzvalene (**59**). The rearrangement proceeds in S_1 via a prefulvenic biradical TS (**57**) leading to a S_1/S_0 conical intersection,^[146–149] and the ESAA relief of benzene in the S_1 state was considered as the driving force for the isomerization (Figure 15B).^[146]

The irradiation of benzene and simple arenes in nucleophilic solvents was investigated by Kaplan et al.^[150] and by Farenhorst and Bickel^[151] in the 1960s, and it was found to provide substituted bicyclo[3.1.0]hexenes **62** (Scheme 5). Since then, the mechanism and driving force for this peculiar loss of aromaticity in S_0 have been subjects for discussions.^[147] The antiaromaticity of benzene in its S_1 state can in principle be relieved by either of two different pathways. First through the unimolecular rearrangement of S_1 benzene to the prefulvene conical intersection which leads to benzvalene (path *a*, Scheme 5) displayed in Figure 15. In the second route, the increased proton affinity of S_1 benzene,^[152] which is comparable to that of COT in S_0 ,^[146] can facilitate protonation of the excited-state benzene (path *b*) leading to the formation of a benzenium

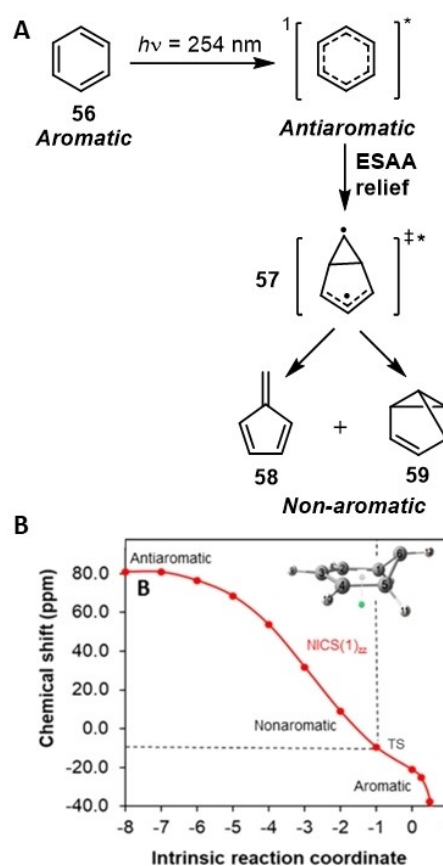
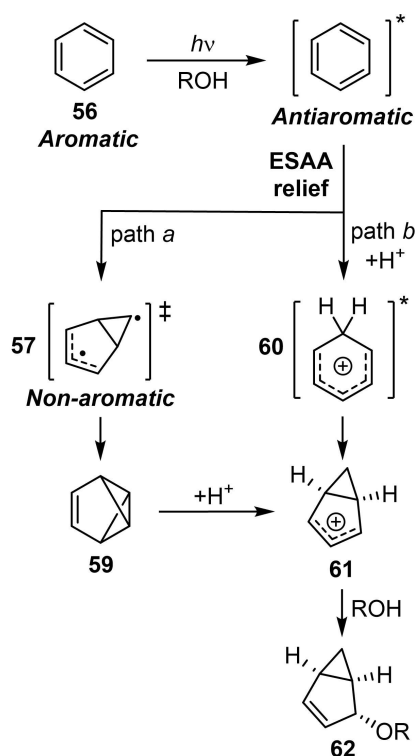


Figure 15. A) Photoisomerization of benzene at 254 nm and B) change in (anti-)aromaticity along the reaction coordinate as given by $\text{NICS}(1)_{zz}$. Reproduced from ref. [146], which is an open access article distributed under the terms of the Creative Commons CC BY license.



Scheme 5. Two possible mechanisms for the formation of bicyclo[3.1.0]hexene derivatives from a benzene photorearrangement in acidic nucleophilic media (ROH).

cation. While both routes provide for ESAA relief, fluorescence quenching and isotope labeling experiments ruled out pathway *b*. The preference of intramolecular rearrangement (path *a*) over intermolecular protonation was explained by the exceedingly low concentration of excited-state benzene (at the conditions used, for example, light intensity, $[S_1\text{-state benzene}] = 10^{-13}$ M) caused by its short lifetime and the relatively low concentration of available protons which favors unimolecular rearrangements (see below).

This photochemical rearrangement is, however, quite non-selective for mono- and polysubstituted arenes,^[153] and the primary photoproducts undergo a number of further reactions,^[154–156] which limit the synthetic utility. However, the isoelectronic pyridinium ions were found to photo-rearrange to the analogous bicyclic products (**66**, Figure 16A), also upon relief of ESAA (Figure 16B).^[157] This rearrangement has been shown to be much more synthetically useful as it can be combined with acid-promoted ring opening of the strained bicyclic product to give various amino-substituted cyclopentenes,^[158] a powerful stereoselective method that has become important in synthesis of biologically active compounds^[159] and other targets.^[160,161]

Similar ESAA triggered photochemistry was observed for pyrylium salts (**67**)^[162] and a silabenzene kinetically stabilized by a very bulky Tbt substituent at Si (**70**; Tbt = 2,4,6-tris[bis(trimethylsilyl)methyl]phenyl)^[163,164] (Figure 17). In the case of **67**, the oxygen atom is incorporated in the three-membered ring, while

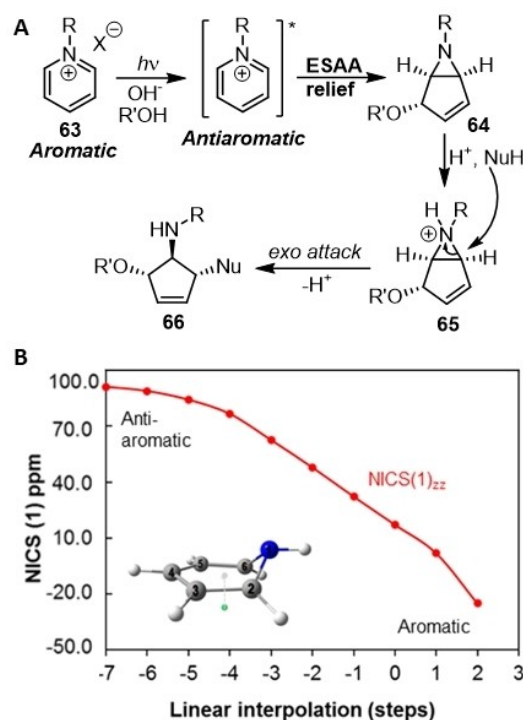


Figure 16. A) Photoisomerization of pyridinium salts and B) change in (anti-)aromaticity along the reaction coordinate as given by NICS(1)_{zz}. Reproduced from ref. [46], which is an open access article distributed under the terms of the Creative Commons CC BY license.

70 rearranges with the bulky Si(Tbt) moiety as a part of the five-membered ring. However, the synthetic utility of these reactions is much lower than that of the corresponding photo-reaction of the pyridinium ions. Noteworthy, the antiaromatic character of **70** in its S_1 state is significantly weaker than that of benzene and the pyridinium ion (see NICS(1) at the S_1 minima, Figures 15B–17B), explained by the weaker SiC than CC π -bonds.^[165]

6.2. Other modes of photochemical reactivity of arenes

Even though reaction path *a* instead of path *b* is followed to product **62** when benzene is irradiated in nucleophilic media (Figure 15), the proton affinity of benzene in S_1 as measured by ion cyclotron resonance spectroscopy is notably higher than in the S_0 state (207.4 vs. 181.4 kcal mol⁻¹).^[152] This feature connects to the relief of S_1 state antiaromaticity through protonation as a nonaromatic benzenium cation is formed in which the cyclic conjugation is disrupted by a sp^3 -hybridized C atom. Such ESAA relief was verified by a large reduction in the NICS(1)_{zz} value upon protonation ($\Delta\text{NICS}(1)_{zz} = -55.6$ ppm). Interestingly, the benzenium cation (**60**) which is formed in the S_1 state puckers to a structure with a short through-space C–C distance of 2.099 Å.^[166] This structure resembles homoaromatic cations such as the homotropylium cation explored extensively in the S_0 state and in which there are one or several through-space interactions along an aromatic cycle.^[167–169]

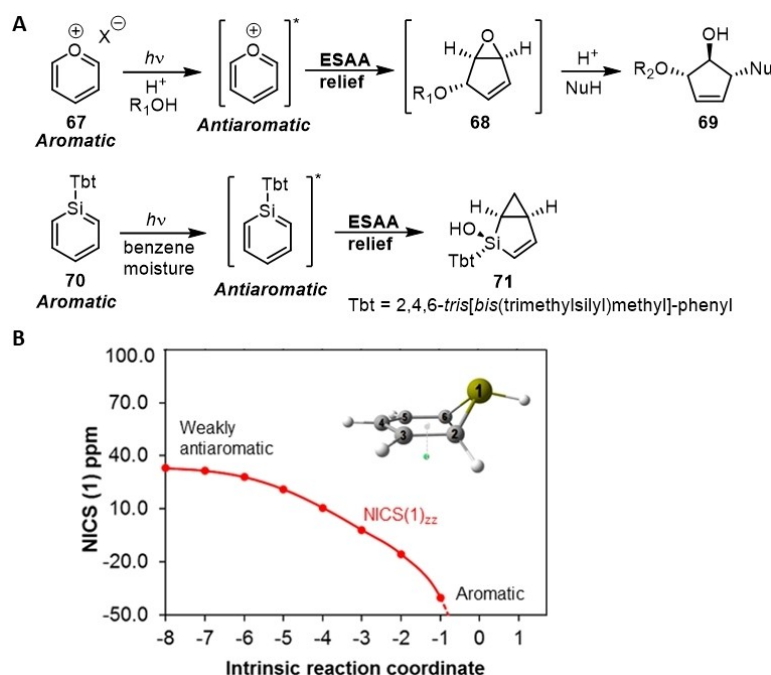


Figure 17. A) Generalized photoisomerization of pyrylium salts and silabenzene and B) change in (anti-)aromaticity along the reaction coordinate for silabenzene photorearrangement as given by NICS(1)_{zz}. Reproduced from ref. [146], which is an open access article distributed under the terms of the Creative Commons CC BY license.

Similarly, both the 10 π -electron cyclooctatetraene dianion (72)^[170] and the cyclononatetraenide anion (77)^[171] are experimentally more easily protonated upon excitation than in the S_0 states, and this should involve the relief from ESAA. Simultaneously, these protonations lead to formation of the homoaromatic 8 π -electron cyclooctatrienyl anion and cyclononatetraene, respectively (Figure 18). The excited-state homoaromatic

characters of these latter species were examined based on various aromaticity indicators including C...C homoconjugative distances ($r(C\cdots C)$), ACID plots, NICS scans and ISE values in the T_1 state, and $r(C\cdots C)$ in the S_1 state. In general, this Baird homoaromaticity should provide extra stabilization to photochemical reaction intermediates,^[172] and similar through-space conjugation leading to excited-state homoaromaticity has been

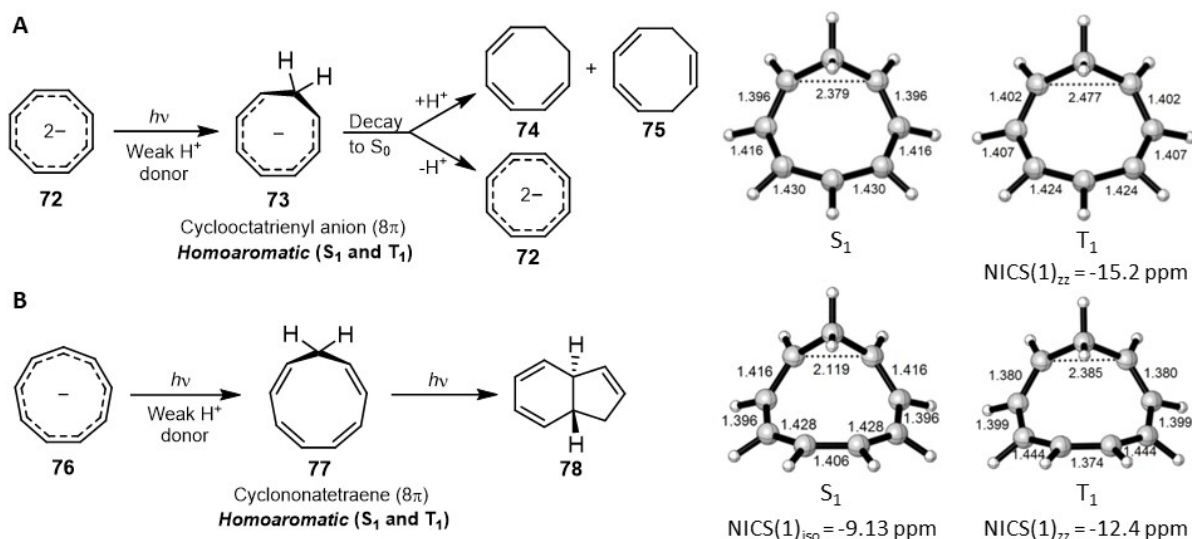


Figure 18. Formation of the homoaromatic 8 π -electron A) cyclooctatrienyl anion and B) cyclononatetraene from photoinduced protonation with evaluations of their homoaromaticity. Reproduced with permission from ref. [172], which is an open access article distributed under the terms of the Creative Commons CC BY 3.0 license.

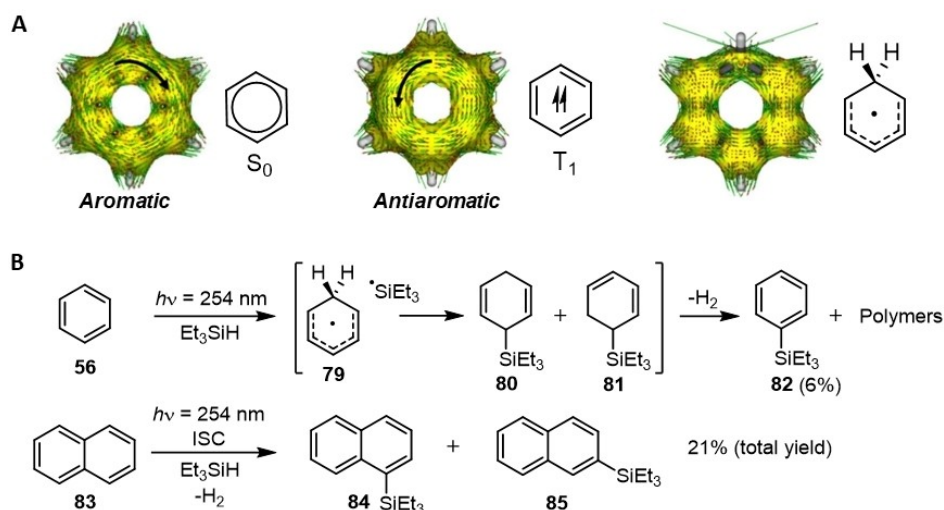


Figure 19. A) Aromaticity evaluation (ACID) of the benzene photohydro-silylation process. B) Photohydro-silylation reactivity of benzene and naphthalene. Reproduced from ref. [102], which is an open access article distributed under the terms of the Creative Commons CC BY license.

used to rationalize computational findings on exciplex formation in the T_1 states of benzene, naphthalene and anthracene.^[173,174]

In addition to protonation, the ESAA character of benzene in T_1 can be diminished through hydrogen atom abstraction from triethylhydrosilane by benzene as also this breaks the cyclic π -conjugation (Figure 19A).^[102] Thus, Baird-antiaromatic $[4n+2]$ annulenes should be susceptible to photochemical addition reactions (cf. Figure 5). Indeed, experimental photohydro-silylation of differently sized arenes (e.g., benzene and naphthalene), using triethylhydrosilane as a heavy “dihydrogen”, was found to successfully afford the corresponding monosilylated products (Figure 19B). It is a two-step process where a T_1 -state arene abstracts a hydrogen atom from the hydrosilane to form the benzenium radical (79) and silyl radical, which then combine to afford silylcyclohexadiene intermediates (80 and 81). Subsequently, they form the final silylated product or polymers and release H_2 gas. The activation barrier of the hydrogen atom abstraction from trimethylhydrosilane was found to be very low for T_1 state benzene (2.4 kcal mol^{-1} with UB3LYP-D3(BJ)/6-311+G(d,p)), much lower than that in the S_1 state (20 kcal mol^{-1} with CASPT2//CASSCF), suggesting that the experimental photosilylation occurs in the T_1 state.

For polybenzenoid aromatic hydrocarbons (PBHs), the reactivity decreased extensively; while benzene reacted to completion by primarily forming polymers, naphthalene only reacted to 21% with the remaining portion unreacted.^[102] Transfer photohydrogenation of a few PBHs (e.g., phenanthrene and anthracene) using formic acid was also observed resulting in their dihydro-derivatives, and although the yields were minute (3-5%) it supports the enhanced photoreactivity of Baird-antiaromatic compounds. In some of the PBHs one could see in the computations that the Baird antiaromaticity localized to certain rings, and these were also the more photoreactive. Indeed, the relative stability of PBHs with angular versus linear three-ring segments in the S_0 and T_1 states is related to the

photoinduced change of aromaticity pattern.^[175,176] Phenacenes are more stable than acenes in the S_0 state due to their larger aromaticity. When the number of fused rings is no more than 12, the stability trend is reversed in the T_1 state, that is, acenes become more stable than phenacenes. Very recently, Baird presented a qualitative theoretical rationalization of this observation,^[177] based on the results from Markert et al.^[175]

Triplet state reactivity of substituted chlorobenzene was recently explored computationally by Nitu and Crespi.^[178] The excited-state antiaromaticity was found to be relieved by puckering (Figure 20), whereupon one unpaired triplet spin localizes on the carbon attached to the chlorine atom, in line with what has been observed earlier by Baranac-Stojanovic.^[126] The resultant species have varied reactivity depending on their further substitution; electron-rich chlorobenzenes favor the radical reduction (Figure 20A), while electron deficient species undergo solvolysis through a photo- S_N2Ar reaction (Figure 20B). Both processes were found to be energetically comparable to,

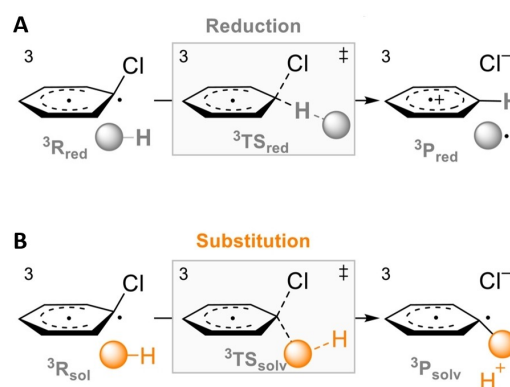
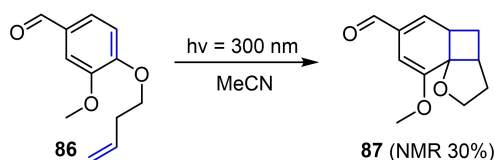


Figure 20. Proposed mechanisms for the A) reduction and B) substitution (S_N2Ar) of triplet aryl chlorides. Reproduced with permission from ref. [178]. Copyright: 2022, Wiley-VCH Verlag GmbH & Co. KGaA.



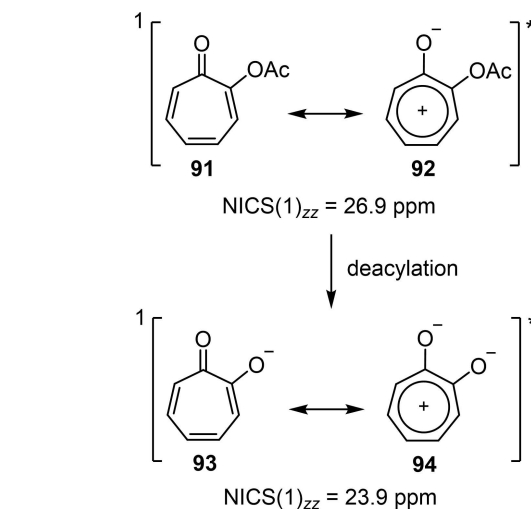
Scheme 6. Intramolecular [2 + 2] photocycloaddition of vanillin.

or more favorable, than the commonly accepted mechanism of photoreactivity, that is, the dissociation of the C–Cl bond to form triplet or singlet aryl cations.

Photochemical cycloadditions of lignin-derived phenol compounds with alkenes (**86**, Scheme 6) can also be considered to be driven by ESAA relief of the S_1 state benzene ring with the formation of photochemically more stable structure.^[179] Under irradiation, vanillin carrying an alkene side chain can undergo intramolecular [2 + 2] photocycloaddition to form a nonaromatic tricyclic product **87**.

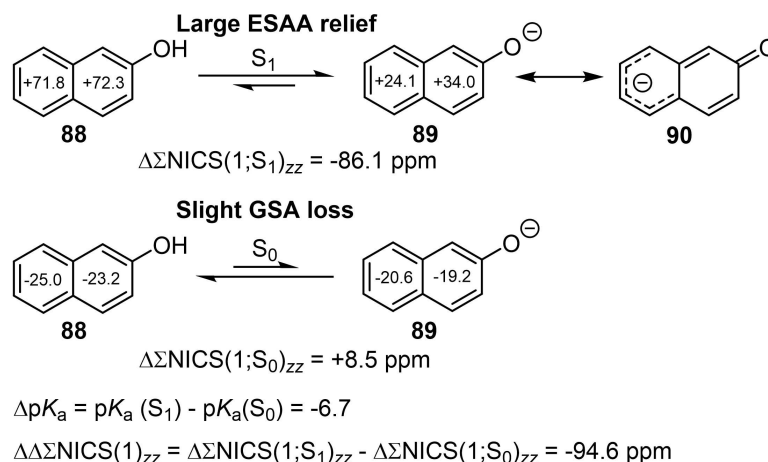
6.3. Photoacidity and ESIPT processes

Photoexcitation also has an impact on the acid-base properties of arene derivatives in their lowest excited states. For compounds that act as photoacids, it has been shown that ESAA relief increases the acidity in the S_1 state when compared to the S_0 state, and thereby drives the deprotonation. For example, 2-naphthol (**88**, Scheme 7) exhibits a considerably enhanced acidity upon excitation ($pK_a = 9.5$ in S_0 and $pK_a^* = 2.8$ in S_1).^[180] The deprotonation can be connected with ESAA relief,^[12] where **88** in the S_1 state was found to be much more antiaromatic than naphthalen-2-olate (**89**) with $\Delta\Sigma\text{NICS}(1)_{zz} = -86.1$ ppm.^[181] The situation is opposite in the S_0 state where the deprotonation instead leads to a slight loss in aromaticity ($\Delta\Sigma\text{NICS}(1)_{zz} = +8.5$ ppm). In the S_1 state, also protic solvent molecules assist in the ESAA alleviation in phenol derivatives as found in a combined spectroscopic and computational study of water-

Figure 21. Effect of tropolone acetate deacylation on ESAA, with NICS calculated in the T_1 state at optimized S_1 state geometries.^[183]

propofol (2,6-diisopropyl-phenol) aggregates with up to eight water molecules.^[182] It was found that not only the phenolic O–H bond is weakened in the excited state but an interaction between water molecules and the benzene ring of propofol also induces a distortion of the molecule to a puckered prefulvenic conformation, a factor that provides for further ESAA alleviation.

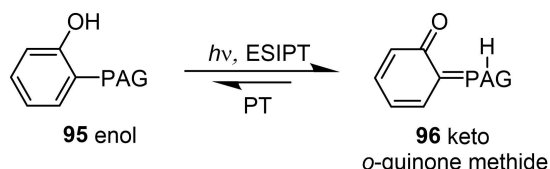
An influence of excited-state antiaromatic character has also been found in tropolone acetate which is deacylated to the tropolonate ion in a catalytic process, accelerated by irradiation with blue LED light.^[183] The tropolone acetate is antiaromatic in the excited-state ($\text{NICS}(1)_{zz} = 26.9$ ppm calculated in the T_1 state at the S_1 state geometry), and the deacylation step is accompanied with a slight relief of ESAA (Figure 21), although much smaller than in case of deprotonation of excited 2-naphthol. The overall catalytic cycle (not shown) was found to

Scheme 7. Deprotonation of 2-naphthol in the S_0 and S_1 states, the $\Delta pK_a = pK_a$ value in the S_1 state minus that in the S_0 state, $\Delta\Sigma\text{NICS}(1)_{zz} = \text{sum of NICS}(1)_{zz}$ values of the two hexagons of the conjugate base minus that of the acid.^[181]

efficiently promote the photochemical acylation of different phenols and alcohols.

Enhanced deprotonation driven by relief of ESAA can also be used to rationalize the photochemical formation of *ortho*-quinone methides **96** (*o*-QMs) through excited-state intramolecular proton transfer (ESIPT) processes. *o*-QMs are highly reactive intermediates in reactions involving phenol derivatives, and they can act as electrophiles and as dienes in pericyclic reactions.^[184] An important example of *o*-QMs precursors are phenolic compounds that undergo ESIPT from an OH group to an adjacent proton-accepting group (PAG; e.g., an imine N atom, a carbonyl O atom, or an sp^2 -hybridized C atom) leading to the formation of a photochromic keto-enol tautomer pair (Scheme 8).

The connection between ESIPT processes and ESAA relief was explored computationally in salicylic acid and 2-(2'-hydroxyphenyl)benzoxazole (HBO) derivatives.^[185–188] Lampkin et al. especially observed that a greater S_0 aromaticity leads to greater S_1 antiaromaticity, a feature that can be used for ESIPT fluorophore design.^[185] In salicylic acid the benzene ring



Scheme 8. The process of ESIPT keto-enol transformation with a proton-accepting group (PAG).

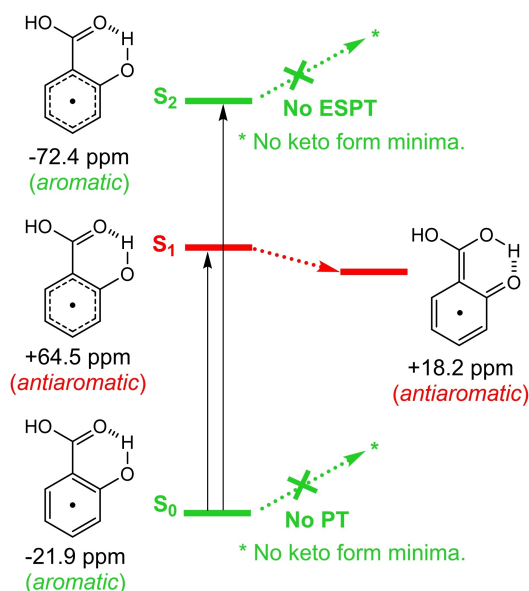
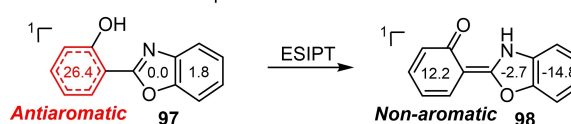


Figure 22. Occurrence of excited-state intramolecular proton transfer (ESIPT) and aromaticity evaluation (NICS(1)_{zz}) of salicylic acid in the S_0 , S_1 , and S_2 states. Reproduced from ref. [186], which is an open access article distributed under the terms of the Creative Commons CC BY license. The general term excited-state proton transfer (ESPT) is used in the figure as it also can be intermolecular. Note that the color scheme is the same as that of Figure 16, and thus, opposite to that of the original figure.

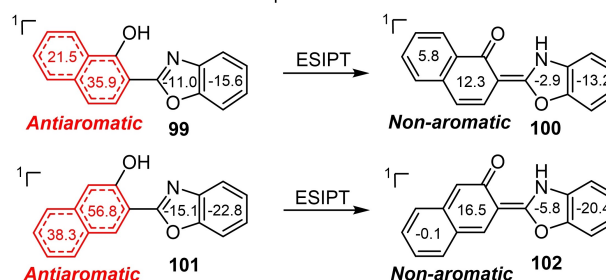
becomes antiaromatic upon excitation to S_1 as its NICS(1)_{zz} value changes from -21.9 ppm in S_0 to $+64.5$ ppm in S_1 . The keto form in S_1 , on the other hand, is much less antiaromatic (NICS(1)_{zz} = $+18.2$ ppm), manifesting the ESAA relief. Interestingly, in the S_2 state the benzene ring was found to be aromatic, and as a result, the ESIPT process in this state is unfavorable (Figure 22).^[186] At this point it should be stressed that it has been concluded that by considering only the (anti-)aromatic character of excited-state reactants and products in ESPT reactions one may neglect important (anti-)aromaticity effects along the reaction paths which are decisive.^[188] This is especially critical when there is an interaction between two electronically excited states.

The ESIPT of HBO (**97**) was also found to be related to ESAA relief. The phenolic ring is aromatic in S_0 (NICS(1)_{zz} = -20.8 ppm) but becomes antiaromatic in S_1 (NICS(1)_{zz} = $+26.4$ ppm, Figure 23). Upon formation of the keto tautomer by ESIPT, the ring becomes nonaromatic (NICS(1)_{zz} = $+12.2$ ppm).^[186] In the HBO system, benzannulation at different positions of the phenolic benzene ring, leading to 2-(2'-hydroxynaphthalenyl)benzoxazole (HNBO; **99** and **101**), can cause either a red- or a blue-shift in the fluorescence. This feature can be rationalized by different magnitudes of the ESAA effect. The S_1 keto tautomer with more Clar sextets in the naphthol moiety is more antiaromatic and therefore alleviates more energy when relaxing to S_0 , leading to a shorter emission wavelength. Thus, benzannulation can be applied as a tool for tuning the magnitude of Stokes shift.^[185,186] On the other hand, benzannulation at the benzoxazole part of HBO, leading to 2-(2'-hydroxyphenyl)naphthoxazole (HNO, **103**), has a smaller impact on the emission energy and leads to a higher proton

HBO: ESAA alleviation from phenol



HNBOs: ESAA alleviation from naphthol



HNO: ESAA alleviation from naphthoxazole

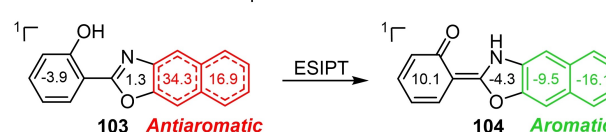


Figure 23. ESIPT of benzannulated HBO in S_1 with aromaticity evaluation (NICS(1)_{zz} values in ppm) of each ring.^[186,187]

transfer energy barrier in the S_1 state.^[187] Studies by NICS(1)_{zz} show that in S_1 , only the naphthol part is antiaromatic in the HNBO enols, while in the HNO enol only the heterocyclic moiety is antiaromatic, that is, ESAA alleviation by ESIPT takes place in different parts of the molecules (Figure 23) as the photo-excitation localizes at the moiety with the longest conjugation, that is, naphthol in HNBO and naphthoxazole in HNO, leading to their aromaticity loss in S_1 .

In a qualitative theoretical study of 58 ESIPT processes, Aihara and co-workers found that ES(A)A plays an important role in ESIPT reactions of phenolic compounds.^[189] Topological resonance energies (TREs) of the S_0 and S_1 states, obtained by Hückel MO theory, of various enol species and their corresponding keto tautomers were compared (Figure 24). Here, positive TRE values indicate stabilization (aromaticity) and negative values destabilization (antiaromaticity) relative to a non-conjugated reference. For almost all keto-enol type ESIPT processes, the relative magnitude in the (anti-)aromatic (de)stabilization between the two isomers was opposite in S_1 as compared to S_0 . That is, in S_0 the enols have positive TREs, and thus, are more conjugatively stabilized (aromatic) than their keto tautomers. In contrast, in S_1 , the TREs of most enols become smaller (regardless of sign) than those of the corresponding keto tautomers, indicating that enols in their S_1 states are less aromatic than the corresponding keto tautomers (Figure 24).

The qualitative TRE and TRE* values of the excited-state keto-enol tautomerization of salicylideneaniline are also in line with results from high-level quantum chemical calculations by Rocha-Rinza and co-workers (Figure 25).^[190] They reported the salicylideneaniline (**109** and **110**) enol-keto tautomerization in the S_1 state to be a barrierless pathway. They used θ' as aromaticity index, where θ' measures the deviation between the electron delocalization in a given cyclic structure and

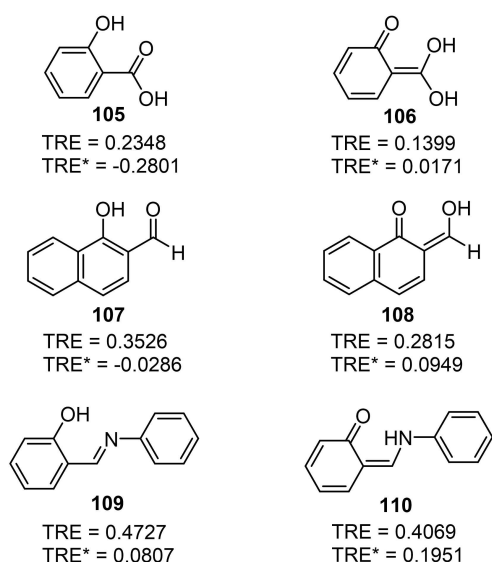


Figure 24. The general process of ESIPT keto-enol transformation and two examples (salicylic acid and salicylideneaniline) of calculated TREs ($|\beta|$) in the S_0 (TRE) and the S_1 (TRE*) states. A positive TRE corresponds to a stabilized (aromatic) and a negative TRE to a destabilized (antiaromatic) situation compared to a nonconjugated reference.^[189]

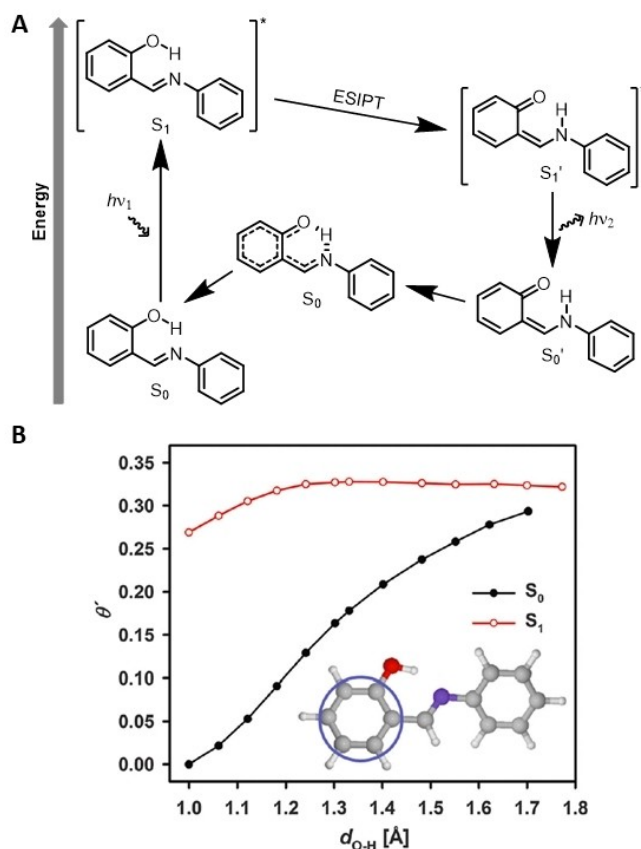
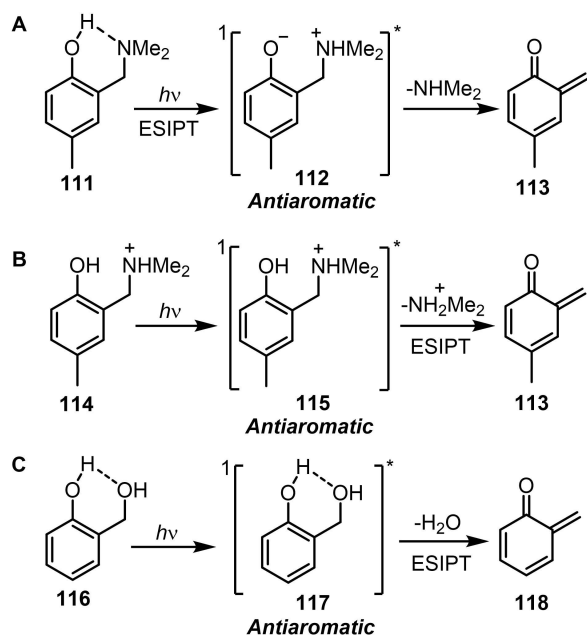


Figure 25. A) The ESIPT mechanism of salicylideneaniline, and B) aromaticity evaluation using the electronic aromaticity index θ' for the encircled phenolic benzene ring along the reaction coordinate from the enol to the keto isomer of salicylideneaniline in the S_0 and S_1 states. The aromatic character of a given ring is lowered with increasing values of θ' . Reproduced with permission from ref. [190]. Copyright: 2015, The Royal Society of Chemistry.

benzene, and found a notable loss of aromaticity in the phenolic benzene ring of **109** upon excitation (Figure 25B). It was concluded that the aromaticity loss induces a redistribution of electron density that drives the proton transfer and tautomerization.

The photochemical formation of the keto-forms can also be step-wise as found for 2-aminomethyl-*p*-cresol (**111**) which upon photoexcitation rapidly undergoes hydrogen bond-mediated ESIPT to form a spectroscopically detectable zwitterionic intermediate, followed by deamination affording the *o*-QM (Scheme 9A).^[191] Similarly, photoexcited 2-aminomethyl-*p*-cresol ammonium (**114**)^[192] and salicyl alcohol (**116**)^[193] rearrange to *o*-QM by ESIPT with deamination and dehydration, respectively, yet in the latter two reactions no zwitterionic intermediate was detected (Scheme 9B and C). For these transformations, the (anti-)aromaticity change along the S_1 PES was not explored and it is unclear at which step the ESAA relief is largest. A number of transformations resembling the ESIPT reactions, and which can be described as photochemical sigmatropic [1,5]-H-shifts, were also proposed to proceed by ESAA relief by Rosenberg et al.^[13,194–196] Several of these photoreactions were

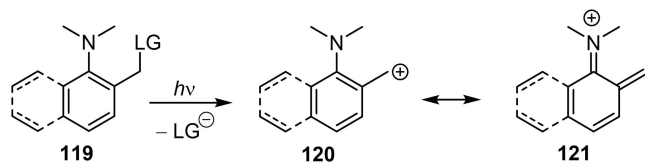


Scheme 9. o-QM formation from A) and B) photodeamination and C) photodehydration.^[191–193]

explored by Löfås et al. as basis for the design of novel optical conductance switches.^[197]

A similar photoreaction was recently concluded to occur in the aminonaphthalene and aminoaniline photocages (119) by Basarić and co-workers (Scheme 10).^[198] The antiaromatic character of the singlet excited state of these molecules drives the heterolysis of the C–LG bond leading to the cleavage of carboxylate and the formation of a carbocation that has a significant contribution of the quinoid structure with the positive charge on the nitrogen, which releases its antiaromatic character.

Proton transfer of 2-methoxy-6-methylacetophenone (122) to its enol form (enolization) can be accelerated by photo-



Scheme 10. Photorelease from aminonaphthalene and aminoaniline photocages. LG: carboxylate.

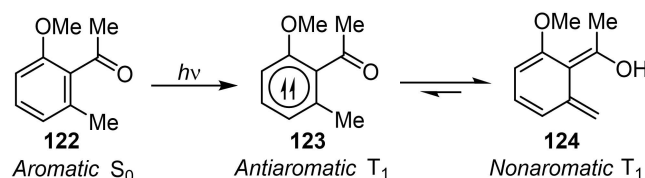


Figure 26. Photoenolization of 2-methoxy-6-methylacetophenone.

excitation (photoenolization) as shown in a computational study by Halder and co-workers (Figure 26).^[199] In the S_0 state the proton transfer energy barrier is $38.2 \text{ kcal mol}^{-1}$, which becomes much smaller ($3.7 \text{ kcal mol}^{-1}$) in the T_1 state. This barrier lowering is explained by the aromaticity change of the phenyl ring in 2-methoxy-6-methylacetophenone. To undergo proton transfer in S_0 , the aromatic reactant ($\text{NICS}(1)_{zz} = -24.4 \text{ ppm}$) has to go through a less aromatic transition state ($\text{NICS}(1)_{zz} \approx -13 \text{ ppm}$), which contributes to the high energy barrier. However, upon photoexcitation and intersystem crossing to the T_1 state, the S_0 -aromatic phenyl ring becomes Baird antiaromatic ($\text{NICS}(1)_{zz} = 26.1 \text{ ppm}$ in the FC region, 7 ppm at the optimal T_1 geometry). At the TS for proton transfer it becomes stabilized by regain in aromaticity ($\text{NICS}(1)_{zz} \approx -22 \text{ ppm}$), and thus, the barrier is significantly lowered.

6.4. Photoswitching

As indicated just above, building on the switch in aromaticity and antiaromaticity when going from the S_0 to the S_1 and T_1 states, for the design of photoswitches is an apparent path. The ESAA character of an annulated benzene ring has been used by Durbbeej, London and co-workers in Irie-type dithienylethene photoswitches^[200,201] which have the ethene-type linker (typical in these switches) replaced by a benzene linker which transforms to an o-xylylene moiety upon irradiation (Figure 27A).^[202] A similar dithienylethene photoswitch with a tetrafluorinated benzene linker was also examined spectroscopically.^[203] According to NICS, HOMA and the electronic Shannon index, the benzene linker becomes antiaromatic at the FC region (Figure 27B), yet this antiaromaticity is relieved when the CI region, where the two thienyl rings become covalently bonded, is approached. This ESAA relief was also quantified using FC relaxation energy differences based on ISE values. In a follow-up study on three different dithienyl-substituted switches with benzene, cyclohexene or CBD π -linkers, it was found that the 6π -electron linker, compared to cyclohexene-linked reference molecule, relieves ESAA in an efficient photocyclization while the CBD linked species does not photoswitch.^[204] Still, photo-switching can potentially be based on the formation of a larger excited-state aromatic isomer if that isomer is nonaromatic instead of antiaromatic in the S_0 state. Such a photoswitch was proposed by Löfås et al. based on a central bicyclo[4.2.0]octa-2,4,7-triene unit which photochemically can isomerize to a COT unit, and then reclose thermally.^[197]

6.5. Photochemical benzopentafulvene formation from o-ethynylstyrenes

As seen in Section 4, twisting of aryl olefin bonds is also a means to relieve T_1 ESAA (Figure 9). When this process occurs in more complex molecular structures, it can facilitate further transformations that are of synthetic utility, for example, the stereoelectronically unfavorable 5-exo-dig cyclization of enyne derivatives.^[205] o-Ethynylstyrenes bearing a hydroxymethyl

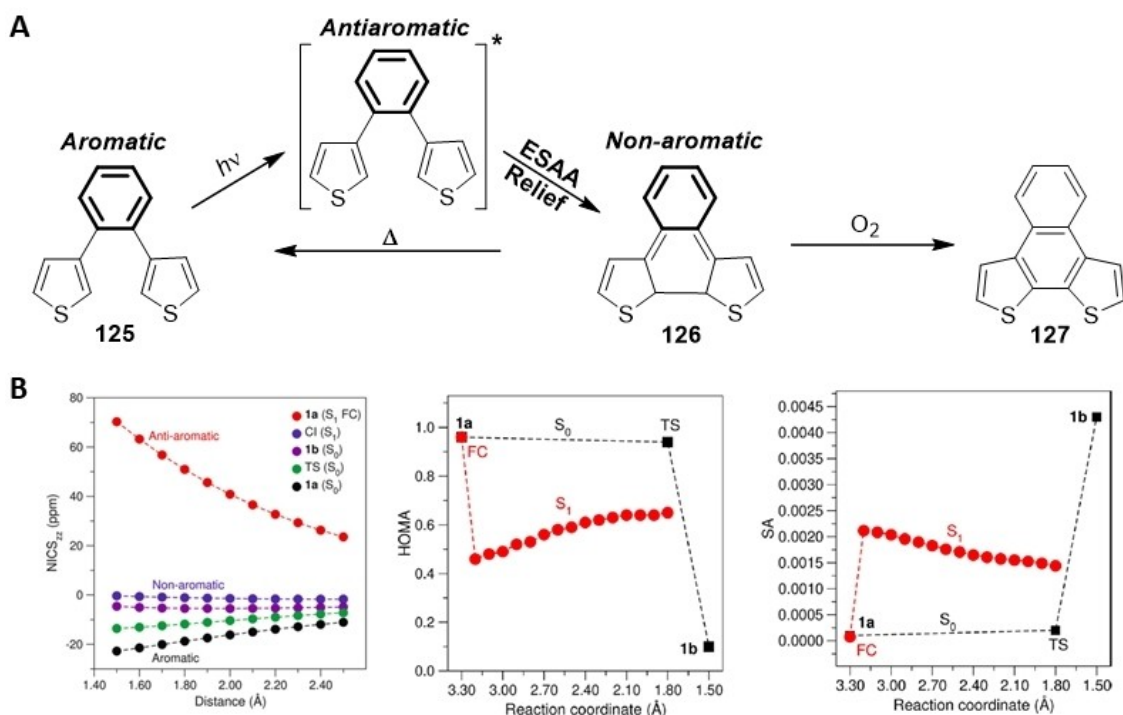


Figure 27. A) Photoswitching of dithienylethene and B) changes in (anti-)aromaticity along the reaction coordinate as evaluated by NICS, HOMA and the Shannon aromaticity (SA) index. Reproduced from ref. [202], an open access article distributed under the terms of the Creative Commons CC BY license.

group on the olefin (128) could be photoexcited to the T_1 state through sensitization, where the S_0 aromatic benzene ring (NICS(1)_{zz} = −24 ppm) turns antiaromatic (NICS(1)_{zz} = +29 ppm). Now, similar to what occurs in simple styrene (Figure 9), the benzene ring reduces its T_1 antiaromaticity by twisting the C=C bond of the olefinic substituent. At the fully 90° twisted structure the olefin bond is best described as a 1,2-biradical while the benzene ring partially regains Hückel aromaticity (NICS(1)_{zz} = −15 ppm, cf. a benzyl radical). At this twisted structure, the C1–C5 cyclization is easily enabled because the radical orbital at the β -carbon of the twisted olefinic π -bond is oriented towards the ethynyl bond (Figure 28). After a subsequent step, which results in formaldehyde elimination, the final benzofulvene product (130) is formed. Importantly, when the central benzene ring is replaced by a cyclohexene ring the reaction does not occur, indicating that T_1 state ESAA relief is the triggering factor for the photochemical benzofulvene formation.

6.6. ESAA relief through electron transfer

A number of recent studies have revealed that a further route for alleviating ESAA is provided by photoionization or photo-reduction leading from the antiaromatic $\pi\pi^*$ state to a formally nonaromatic radical cation or anion, respectively. Photoinduced intramolecular electron transfer, leading to photo-dissociation, occurs in phenyltetrazole^[206] and in reactions with photo-removable protecting groups that contain benzene moieties.^[207]

In the first case, 5-phenyl-2H-tetrazole (131) upon photo-excitation undergoes ring-opening of the tetrazole moiety and release of dinitrogen (Figure 29). The vertical excitation to the S_1 state is primarily localized to the Ph group which becomes strongly antiaromatic (NICS(1)_{zz} = 385.1 ppm) while the tetrazole ring remains aromatic (NICS(1)_{zz} = −59.2 ppm). Yet, an intramolecular electron transfer occurs from the π^* orbital of the Ph group to the π^* orbital of the tetrazole ring which leads to an ESAA of the Ph group turns (NICS(1)_{zz} = 5.0 ppm) followed by cleavage of the N1–N2 bond of the tetrazole, and finally, electron transfer back to the Ph group which restores its Hückel aromaticity (NICS(1)_{zz} = −29.3 ppm).

A similar reaction is the photochemical C–Cl bond dissociation in coumarinylmethyl chloride (135, Figure 30A), where the chloride models a phosphate, carboxylate, sulfate, sulfonate or another group for which the coumarinylmethyl moiety is used as a photoremovable protecting group.^[208,209] Again, the aromatic benzene ring in 135 becomes antiaromatic upon a $\pi\pi^*$ excitation, and as ESAA alleviating mode, the C–C–Cl dihedral angle rotates to a structure with an enhanced overlap between the π^* orbital of the ring and the σ^* orbital of the C–Cl bond which weakens the C–Cl bond. Hückel aromaticity is then regained upon back-electron transfer to the ring. The changes in aromaticity during the process was monitored through a dynamics simulation with NICS(1)_{zz} computed at various times. The vertically excited 135 (1 in Figure 30B) is nearly planar and shows an antiaromatic character of the benzene ring (NICS(1)_{zz} = 24.3 ppm). This ring distorts and at 102 fs it is nonaromatic (NICS(1)_{zz} = 3.5 ppm) due to the electron

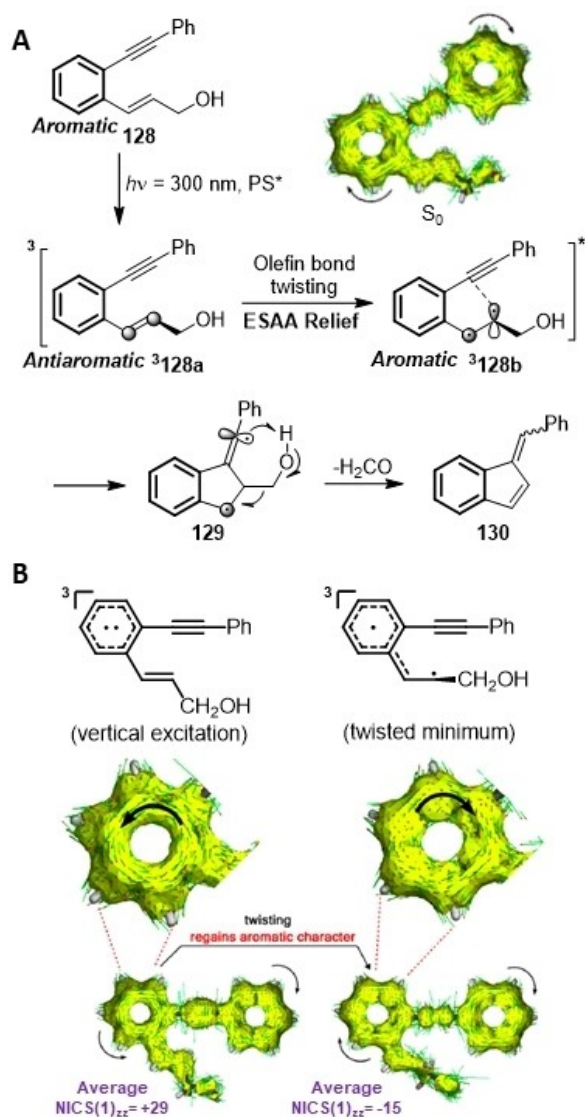


Figure 28. A) Photochemical 5-exo-dig cycloaromatization of *o*-ethynylstyrene (with ACID plot in the S_0 state). B) Aromaticity evaluations ($\text{NICS}(1)_{zz}$ and ACID) of T_1 -state *o*-ethynylstyrene before and after olefin bond twisting. Reproduced with permission from ref. [205]. Copyright: 2015, American Chemical Society.

loss. Again, ESAA relief triggers intramolecular electron transfer from the benzene ring, and thus, the C–Cl bond cleavage.^[207]

Going to larger molecules, ESAA relief can also act as a driving force for ligand-metal charge transfer (LMCT) in different $[26]\pi$ metallohexaphyrins as observed by Kim and co-workers.^[210] In the S_0 state, $[26]\pi$ metallohexaphyrins, bis-gold (137), mono-gold (138), and mono-palladium (139) hexaphyrins (Figure 31A), are aromatic and stable macrocycles with 137 is the most aromatic and 139 the least. Upon photoexcitation to the FC state, it is concluded that their hexaphyrin rings become S_1 antiaromatic and destabilized, in analogy with earlier observations on 1,3-phenylene-bridged $[26]/[28]$ hexaphyrin congeners.^[211] This leads to an intramolecular LMCT process which is most rapid for 137 and slowest for 139 (Figure 31B).

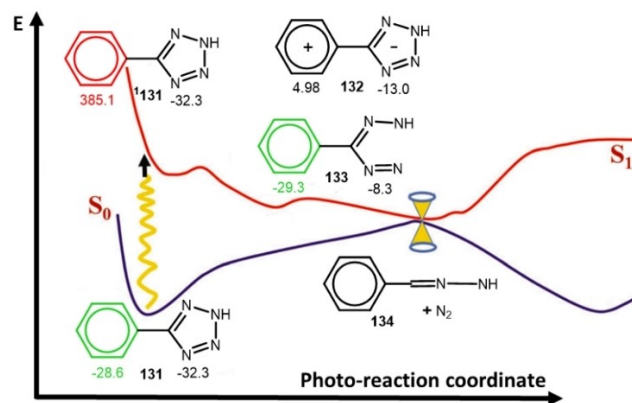


Figure 29. Photoreaction path of 5-phenyl-2H-tetrazole (131) describing the changes in aromaticity ($\text{NICS}(1)_{zz}$) along the reaction coordinate, with permission. Parts reproduced with permission from ref. [206]. Copyright: 2016, The Royal Society of Chemistry.

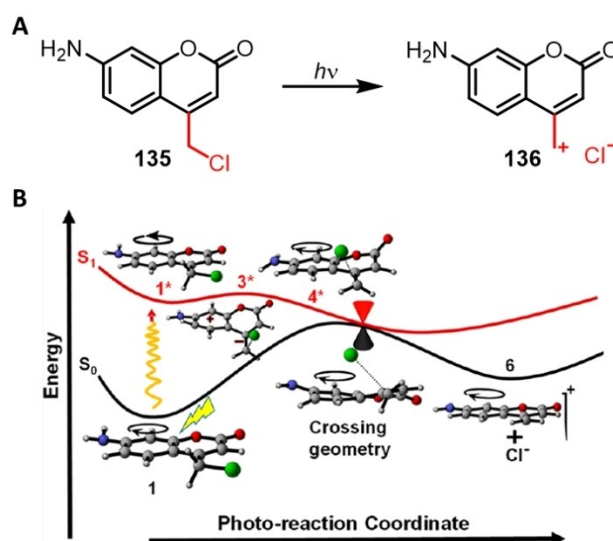


Figure 30. A) Photocleavage of coumarinylmethyl chloride, and B) S_0 and S_1 PESs of the process and conformational change. Note that compounds 135 and 136 in (A) are labeled 1 and 6 in (B). Reproduced with permission from ref. [207]. Copyright: 2020, American Chemical Society.

This resulted in a decreased electron density on the hexaphyrin ring, whereby the electron withdrawal by the perfluorophenyl substituents (C_6F_5 , Ar in Figure 30A) from the hexaphyrin ring was attenuated. This led to a strong blue-shift in the IR frequencies of the Ar groups (from 1450–1550 to 1510–1530 cm^{-1}) in time-resolved IR absorption spectrum, a secondary effect which reflects the ESAA relief.

Photoinduced electron transfer can also occur between molecular entities in supramolecular structures, with the most well-known being the photo-deactivation of Watson-Crick adenine (A)-thymine (T) and guanine (G)-cytosine (C) base pairs in DNA.^[212] This photo-deactivation proceeds by proton coupled electron transfer (PCET), also known as electron-driven proton transfer (EDPT), from the photoexcited purines A/G (A^*/G^*) to the corresponding pyrimidines T/G. The ultrafast PCET process

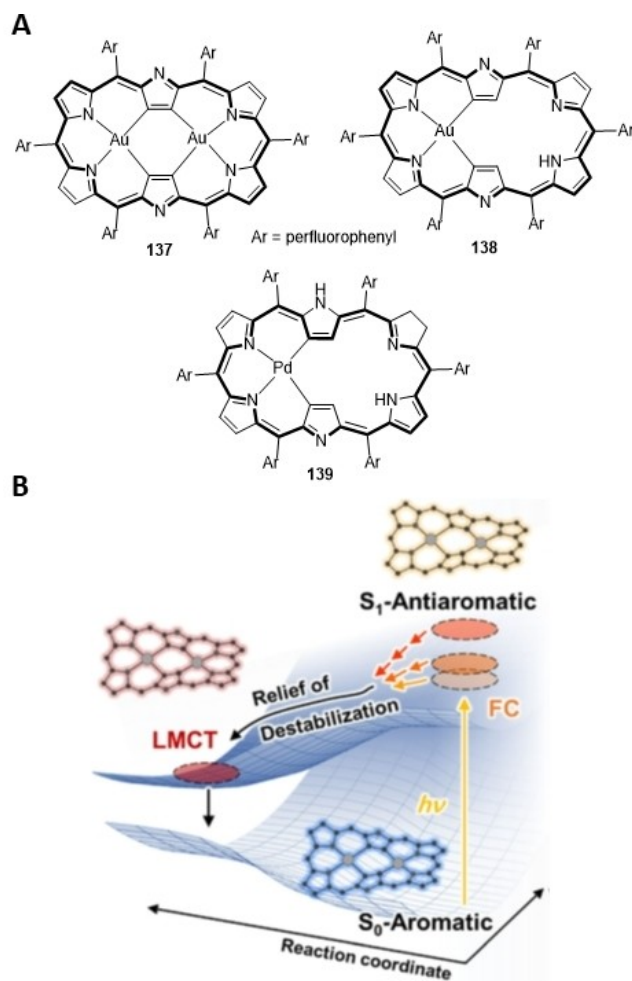
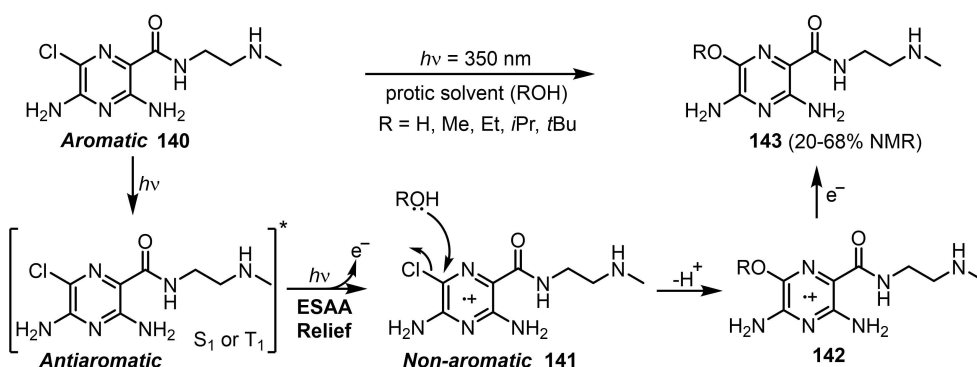


Figure 31. LMCT process of 137, 138 and 139 driven by relief of ESAA. A) Structures of 137, 138 and 139. B) Suggested PES plot of the LMCT process. Reproduced with permission from ref. [210]. Copyright: 2022, Wiley-VCH Verlag GmbH & Co. KGaA.

is barrierless and can be linked to alleviation of ESAA (Figure 32),^[212] providing information on the PCET process which is complementary to the Rehm-Weller model telling that the excited-state electron-transfer rates correlate with the S_0 -state

redox potentials of the electron donating and accepting moieties.^[213,214] According to the new model, the S_0 aromatic purine rings upon photoexcitation to the locally excited $^1\pi\pi^*$ state become highly antiaromatic and rapidly transfer a π -electron to the σ^* orbital of N–H bond, which subsequently cleaves homolytically leading to a proton transfer to the pyrimidine. In this way, the purines relieve photoinduced antiaromaticity and regain aromaticity that stabilizes the charge-transfer state (CT), whereas the weakly aromatic pyrimidines turn slightly antiaromatic (Figure 32). Importantly, the ESAA relief model was demonstrated to be in line with the S_0 -state Rehm-Weller model. For example, the more antiaromatic A ($\Sigma\text{NICS}(1)_{zz} = +58.1$ ppm) and G ($\Sigma\text{NICS}(1)_{zz} = +140.6$ ppm), compared with their 1,3-hydrogen shifted isomers (respectively, $\Sigma\text{NICS}(1)_{zz} = +44.9$ and $+72.0$ ppm), have lower vertical ionization potentials (IP) in the $^3\pi\pi^*$ states, and thus, more easily lose an electron.

Finally, photoinduced intermolecular electron transfer triggered by ESAA can also go to the surrounding medium as observed for amiloride derivatives **140** (Scheme 11),^[215] a class of diuretic drug compounds. Upon irradiation, amilorides undergo photosubstitution in various protic solvents.^[216–220] The reaction was explored by Jorner et al. in a combined experimental and computational study, revealing a biphotonic mechanism.^[215] In the substitution process, the pyrazine core is first excited by one photon to its $\pi\pi^*$ S_1 state, followed by intersystem crossing to T_1 . A second photon absorbed by the molecule in its T_1 (or S_1) state leads to an electron ejection out of the ring into the solvent whereby an amiloride radical cation intermediate is formed (Scheme 11). A subsequent nucleophilic attack by a solvent molecule (ROH), and final reduction by the solvated electron leads to the observed substituted amiloride derivative **140**. The aromaticity change upon the excited-state ionization in the second step was explored through magnetic and electronic aromaticity indices using a simplified model structure, for which the NICS(1)_{zz} value changes from 22 ppm in the T_1 state to -6 ppm in the radical cation, revealing an ESAA relief.



Scheme 11. Biphotonic mechanism of photosubstitution of amiloride analogue **140** in protic solvents.^[215]

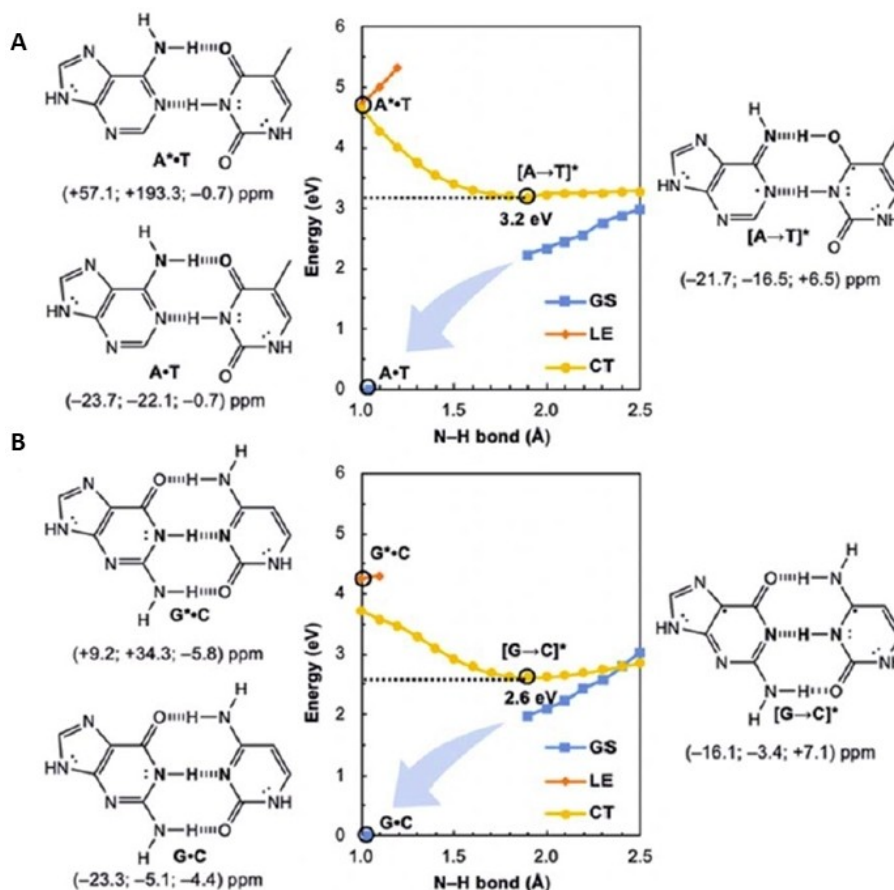


Figure 32. Potential energy functions with constrained N–H bond distance for EDPT processes of Watson-Crick A) A–T and B) G–C pairs in the electronic ground state (GS), $^1\pi\pi^*$ locally excited-state (LE), and charge-transfer state (CT). Reproduced from ref. [212], which is an open access article distributed under the terms of the Creative Commons CC BY 3.0 license.

6.7. Synopsis

As is clear from above, ESAA can trigger a number of processes (Figure 33), the unifying theme being that they all allow the molecule to alleviate this antiaromaticity following the general path described in Figure 8A. If there is an intramolecular path for ESAA relief, and the molecule is conformationally flexible in the excited state, it is likely this path will be followed as it is

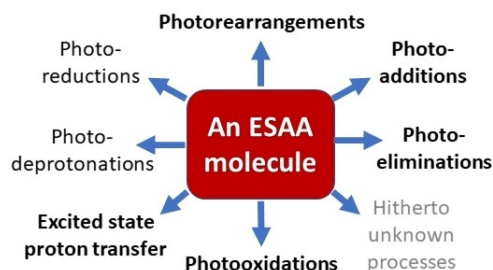


Figure 33. The various processes by which an excited-state antiaromatic molecule can alleviate its antiaromaticity. Processes in bold are discussed in this section, those in normal print in ref. [12]. In gray are photochemical processes waiting to be discovered.

unimolecular. This is exemplified by the T_1 state olefin twist of *o*-ethynylstyrenes with hydroxymethyl groups at the olefin, leading to benzofulvenes through expulsion of formaldehyde.^[205] Molecules which have less flexible structures can instead alleviate the ESAA through a bimolecular reaction. Here, the realization that an excited-state antiaromatic molecule seeks to alleviate this antiaromaticity can allow for development of new photoreactions and improved descriptions of existing ones. It may also provide deepened understanding of photo(in)stability of molecules for environmental or pharmaceutical relevance, and enable us to degrade hazardous chemicals more rapidly as one may identify and enhance conditions that forces the molecule to follow an ESAA triggered degradation pathway. Efforts should be focused on searching for processes of this kind that hitherto are unknown.

7. Conclusions and Outlook

In this review we have described the impact of excited-state aromaticity and antiaromaticity on the photochemical behavior of different π -conjugated (hetero)annulene derivatives. We first discussed various evidence of how ES(A)A influences the

physical properties of organic molecules (excited-state energies and shapes of potential energy surfaces, Stokes shifts, dipole moments, proton affinities, pK_a values). Focus was placed on how gain of ESA or alleviation of ESAA connects with photoreactivity, and explicit application examples from a range of areas, for example pharmaceutical chemistry, functional organic materials, and biochemistry, were reviewed.

However, it is important to stress that the application of the ES(A)A concept to rationalize photoreactivity is not limited to the photochemical transformations described herein. In general, it can be used as a tool for predicting the stability of molecules in their excited states in applications where high photochemical persistence is required (e.g., fluorescent dyes, photoredox catalysts, organic solar cell materials, and photosensitizers) and where photoreactivity and photobleaching can lead to substantial health and environmental risks (photoinduced degradation of pharmaceuticals and pesticides, for example, chlorpyrifos^[221]). Alternatively, it can provide us with knowledge on how to improve the degradation of environmentally hazardous compounds and materials. It can also prove useful for the design of new photoactivatable molecules whose photoreactivity can be enhanced by ESAA or ESA (photoremovable protecting groups, photoswitches, photoacids, super-resolution microscopy dyes, etc.). Finally, the concepts can likely be used to rationalize several irradiation-induced processes observed in astrochemistry and prebiotic chemistry, as well as numerous other areas, and also used much more in applied areas of chemistry. For instance, striving towards ESA character upon excitation may provide the means to photo-repair partially degraded photoactive materials (e.g., organic materials for photovoltaics and optoelectronics) giving opportunities for improved materials reusability and allowing us to establish circular chemistry processes.^[222]

Yet, despite being a powerful concept, gain of ESA or relief of ESAA always needs to be examined in the context of other known effects influencing the reactivity of excited states, and it should be emphasized that Baird's rule applies to lowest $\pi\pi^*$ states (or $\sigma\sigma^*$ states), not to $n\pi^*$ states. The excitation must be localized to the ring under consideration and not primarily to a (neighboring) functional group such as a carbonyl group. The situation is especially complicated in polycyclic conjugated compounds as a calculated negative NICS value in the T_1 state might not necessarily correspond to Baird-aromatic character; it can instead correspond to Hückel-aromatic character that has shifted from one ring to another upon excitation.^[57,58] There are also molecules that, in their lowest $\pi\pi^*$ excited state, are simultaneously Hückel and Baird aromatic, that is, they are Hückel-Baird-hybrid aromatics in those states.^[50,51] The analysis of a potential excited-state aromatic and antiaromatic character should therefore be pursued with caution, and quantitative computation should be combined with a qualitative theoretical analysis and rationalization of the tentative ES(A)A effect (as described in Figure 2). As important as it is to determine the scope, it is equally important to determine the limitations, complications and pitfalls of the concepts. Only then can the concepts become valuable tools in the design and development of molecules for use in various applications.

Taken together, the excited-state aromaticity and antiaromaticity concepts are model concepts that can be very useful (if exercised with care) for the rationalizations of an observed photoreactivity in a range of different areas where light-matter interactions take place.

Acknowledgements

H.O. and J.Y. are grateful to Stiftelsen Olle Engquist Minne (grant 194-0677) for a postdoctoral fellowship to J.Y. and to the Swedish Research Council (grant 2019-05618) for financial support. T.S. acknowledges the INTER-COST grant (no. LTC20076) provided by the Czech Ministry of Education, Youth and Sports and the Czech Science Foundation (project no. 19-20467Y).

Conflict of Interest

The authors declare no conflict of interest.

Data Availability Statement

Data sharing is not applicable to this article as no new data were created or analyzed in this study.

Keywords: antiaromaticity · aromaticity · Baird's rule · excited states · photoreactivity

- [1] J. F. Gonthier, S. N. Steinmann, M. D. Wodrich, C. Corminboeuf, *Chem. Soc. Rev.* **2012**, *41*, 4671–4687.
- [2] V. J. Michl, V. Bonačić-Koutecký, *Electronic Aspects of Organic Photochemistry*, Wiley Chichester, **1990**.
- [3] P. Kimber, F. Plasser, *Phys. Chem. Chem. Phys.* **2020**, *22*, 6058–6080.
- [4] V. I. Minkin, M. N. Glukhovtsev, B. Y. Simkin, *Aromaticity and Antiaromaticity. Electronic and Structural Aspects*, Wiley, New York, **1994**.
- [5] P. von R. Schleyer, *Chem. Rev.* **2001**, *101*, 1115–1118.
- [6] A. T. Balaban, D. C. Oniciu, A. R. Katritzky, *Chem. Rev.* **2004**, *104*, 2777–2812.
- [7] R. Gleiter, G. Haberhauer, *Aromaticity and Other Conjugation Effects*, Wiley, **2012**.
- [8] *Aromaticity: Modern Computational Methods and Applications* (Ed.: F. Israel), Elsevier, **2021**.
- [9] M. Solà, A. I. Boldyrev, M. K. Cyrański, T. M. Krygowski, G. Merino, *Aromaticity and Antiaromaticity: Concepts and Applications*, Wiley, **2022**.
- [10] N. C. Baird, *J. Am. Chem. Soc.* **1972**, *94*, 4941–4948.
- [11] H. Ottosson, *Nat. Chem.* **2012**, *4*, 969–971.
- [12] L. J. Karas, J. I. Wu, *Nat. Chem.* **2022**, *14*, 723–725.
- [13] M. Rosenberg, C. Dahlstrand, K. Kilså, H. Ottosson, *Chem. Rev.* **2014**, *114*, 5379–5425.
- [14] R. Papadakis, H. Ottosson, *Chem. Soc. Rev.* **2015**, *44*, 6472–6493.
- [15] J. Oh, Y. M. Sung, Y. Hong, D. Kim, *Acc. Chem. Res.* **2018**, *51*, 1349–1358.
- [16] C. Liu, Y. Ni, X. Lu, G. Li, J. Wu, *Acc. Chem. Res.* **2019**, *52*, 2309–2321.
- [17] K. Jorner, in *Aromaticity: Modern Computational Methods and Applications* (Ed.: I. B. T.-A. Fernandez), Elsevier, **2021**, 375–405.
- [18] J. Kim, J. Oh, A. Osuka, D. Kim, *Chem. Soc. Rev.* **2022**, *51*, 268–292.
- [19] M. Solà, *Nat. Chem.* **2022**, *14*, 585–590.
- [20] Z. Badri, C. Foroutan-Nejad, *Phys. Chem. Chem. Phys.* **2016**, *18*, 11693–11699.
- [21] R. J. F. Berger, A. Viel, *Zeitschr. Naturforsch. B* **2020**, *75*, 327–339.

- [22] F. Plasser, *Chemistry (Easton)* **2021**, 3, 532–549.
- [23] P. B. Karadakov, S. Saito, *Angew. Chem. Int. Ed.* **2020**, 59, 9228–9230; *Angew. Chem.* **2020**, 132, 9312–9314.
- [24] M. D. Peeks, J. Q. Gong, K. McLoughlin, T. Kobatake, R. Haver, L. M. Herz, H. L. Anderson, *J. Phys. Chem. Lett.* **2019**, 10, 2017–2022.
- [25] I. Casademont-Reig, E. Ramos-Cordoba, M. Torrent-Sucarrat, E. Matito, *Molecules* **2020**, 25, 711.
- [26] R. Ayub, O. El Bakouri, J. R. Smith, K. Jorner, H. Ottosson, *J. Phys. Chem. A* **2021**, 125, 570–584.
- [27] D. Geuenich, K. Hess, F. Köhler, R. Herges, *Chem. Rev.* **2005**, 105, 3758–3772.
- [28] D. Sundholm, H. Fliegl, R. J. F. Berger, *WIREs Comput. Mol. Sci.* **2016**, 6, 639–678.
- [29] G. Monaco, F. F. Summa, R. Zanasi, *J. Chem. Inf. Model.* **2021**, 61, 270–283.
- [30] G. Monaco, R. Zanasi, *J. Phys. Chem. A* **2018**, 122, 4681–4686.
- [31] P. von R. Schleyer, C. Maerker, A. Dransfeld, H. Jiao, N. J. R. van Eikema Hommes, *J. Am. Chem. Soc.* **1996**, 118, 6317–6318.
- [32] H. Fallah-Bagher-Shaidaei, C. S. Wannere, C. Corminboeuf, R. Puchta, P. v. R. Schleyer, *Org. Lett.* **2006**, 8, 863–866.
- [33] A. Stanger, *J. Org. Chem.* **2006**, 71, 883–893.
- [34] R. Gershoni-Poranne, A. Stanger, *Chem. Eur. J.* **2014**, 20, 5673–5688.
- [35] P. Bultinck, S. Fias, R. Ponc, *Chem. Eur. J.* **2006**, 12, 8813–8818.
- [36] S. Van Damme, G. Acke, R. W. A. Havenith, P. Bultinck, *Phys. Chem. Chem. Phys.* **2016**, 18, 11746–11755.
- [37] E. Paenurk, R. Gershoni-Poranne, *Phys. Chem. Chem. Phys.* **2022**, 24, 8631–8644.
- [38] S. Radenković, S. Đorđević, *Phys. Chem. Chem. Phys.* **2021**, 23, 11240–11250.
- [39] L. Zhao, R. Grande-Aztatzi, C. Foroutan-Nejad, J. M. Ugalde, G. Frenking, *ChemistrySelect* **2017**, 2, 863–870.
- [40] P. Preethalayam, N. Proos Vedin, S. Radenković, H. Ottosson, *J. Phys. Org. Chem.* **2023**, 36, e4455.
- [41] T. M. Krygowski, H. Szatyłowicz, O. A. Stasyuk, J. Dominikowska, M. Palusiak, *Chem. Rev.* **2014**, 114, 6383–6422.
- [42] F. Feixas, E. Matito, J. Poater, M. Solà, *Chem. Soc. Rev.* **2015**, 44, 6434–6451.
- [43] P. Bultinck, R. Ponc, S. Van Damme, *J. Phys. Org. Chem.* **2005**, 18, 706–718.
- [44] E. Matito, M. Duran, M. Solà, *J. Chem. Phys.* **2004**, 122, 14109.
- [45] E. Matito, M. Duran, M. Solà, *J. Chem. Phys.* **2006**, 125, 59901.
- [46] D. W. Szczepanik, M. Andrzejak, J. Dominikowska, B. Pawelek, T. M. Krygowski, H. Szatyłowicz, M. Solà, *Phys. Chem. Chem. Phys.* **2017**, 19, 28970–28981.
- [47] J. C. Santos, W. Tiznado, R. Contreras, P. Fuentealba, *J. Chem. Phys.* **2004**, 120, 1670–1673.
- [48] S. Villaume, H. A. Fogarty, H. Ottosson, *ChemPhysChem* **2008**, 9, 257–264.
- [49] E. Matito, *Phys. Chem. Chem. Phys.* **2016**, 18, 11839–11846.
- [50] K. Jorner, F. Feixas, R. Ayub, R. Lindh, M. Solà, H. Ottosson, *Chem. Eur. J.* **2016**, 22, 2793–2800.
- [51] S. Escayola, C. Tonnelé, E. Matito, A. Poater, H. Ottosson, M. Solà, D. Casanova, *Angew. Chem. Int. Ed.* **2021**, 60, 10255–10265; *Angew. Chem.* **2021**, 133, 10343–10353.
- [52] P. v. R. Schleyer, F. Pühlhofer, *Org. Lett.* **2002**, 4, 2873–2876.
- [53] C. S. Wannere, D. Moran, N. L. Allinger, H. B. Andes, L. J. Schaad, P. von R. Schleyer, *Org. Lett.* **2003**, 5, 2983–2986.
- [54] J. Zhu, K. An, P. v. R. Schleyer, *Org. Lett.* **2013**, 15, 2442–2445.
- [55] K. An, J. Zhu, *Eur. J. Org. Chem.* **2014**, 2014, 2764–2769.
- [56] B. Oruganti, J. Wang, B. Durbjee, *Org. Lett.* **2017**, 19, 4818–4821.
- [57] W. Zeng, O. El Bakouri, D. W. Szczepanik, H. Bronstein, H. Ottosson, *Chem. Sci.* **2021**, 12, 6159–6171.
- [58] W. Zeng, D. W. Szczepanik, H. Bronstein, *J. Phys. Org. Chem.* **2023**, 36, e4441.
- [59] Y.-C. Lin, D. Sundholm, J. Jusélius, *J. Chem. Theory Comput.* **2006**, 2, 761–764.
- [60] C. Foroutan-Nejad, *Theor. Chem. Acc.* **2015**, 134, 8.
- [61] C. Foroutan-Nejad, J. Vicha, A. Ghosh, *Phys. Chem. Chem. Phys.* **2020**, 22, 10863–10869.
- [62] D. Buzsáki, M. B. Kovács, E. Humpfner, Z. Harcsa-Pintér, Z. Kelemen, *Chem. Sci.* **2022**, 13, 11388–11393.
- [63] E. Hückel, *Z. Phys.* **1931**, 70, 204–286.
- [64] R. Breslow, J. Brown, J. J. Gajewski, *J. Am. Chem. Soc.* **1967**, 89, 4383–4390.
- [65] M. J. S. Dewar, *Tetrahedron* **1966**, 22, 75–92.
- [66] M. J. S. Dewar, *Angew. Chem. Int. Ed.* **1971**, 10, 761–776; *Angew. Chem.* **1971**, 83, 859–875.
- [67] H. E. Zimmerman, *J. Am. Chem. Soc.* **1966**, 88, 1564–1565.
- [68] J. Aihara, *Bull. Chem. Soc. Jpn.* **1978**, 51, 1788–1792.
- [69] V. Gogonea, P. v. R. Schleyer, P. R. Schreiner, *Angew. Chem. Int. Ed.* **1998**, 37, 1945–1948; *Angew. Chem.* **1998**, 110, 2045–2049.
- [70] M. Saunders, R. Berger, A. Jaffe, J. M. McBride, J. O'Neill, R. Breslow, J. M. Hoffmann, C. Perchonock, E. Wasserman, R. S. Hutton, K. J. Kuck, *J. Am. Chem. Soc.* **1973**, 95, 3017–3018.
- [71] S. Zilberg, Y. Haas, *J. Phys. Chem. A* **1998**, 102, 10851–10859.
- [72] P. B. Karadakov, *J. Phys. Chem. A* **2008**, 112, 12707–12713.
- [73] P. B. Karadakov, *J. Phys. Chem. A* **2008**, 112, 7303–7309.
- [74] P. B. Karadakov, P. Hearnshaw, K. E. Horner, *J. Org. Chem.* **2016**, 81, 11346–11352.
- [75] F. Feixas, J. Vandenbussche, P. Bultinck, E. Matito, M. Solà, *Phys. Chem. Chem. Phys.* **2011**, 13, 20690–20703.
- [76] P. Wan, E. Krogh, *J. Chem. Soc. Chem. Commun.* **1985**, 1207–1208.
- [77] I. McAuley, E. Krogh, P. Wan, *J. Am. Chem. Soc.* **1988**, 110, 600–602.
- [78] D. Budac, P. Wan, *Can. J. Chem.* **1996**, 74, 1447–1464.
- [79] D. Brousmiche, D. Shukla, P. Wan, *Chem. Commun.* **1997**, 709–710.
- [80] D. Shukla, P. Wan, *J. Photochem. Photobiol. A* **1998**, 113, 53–64.
- [81] P. Wan, E. Krogh, B. Chak, *J. Am. Chem. Soc.* **1988**, 110, 4073–4074.
- [82] E. Gaillard, M. A. Fox, P. Wan, *J. Am. Chem. Soc.* **1989**, 111, 2180–2186.
- [83] P. Wan, E. Krogh, *J. Am. Chem. Soc.* **1989**, 111, 4887–4895.
- [84] P. Wan, D. Budac, M. Earle, D. Shukla, *J. Am. Chem. Soc.* **1990**, 112, 8048–8054.
- [85] P. Wan, D. Budac, E. Krogh, *J. Chem. Soc. Chem. Commun.* **1990**, 255–257.
- [86] E. Krogh, P. Wan, *J. Am. Chem. Soc.* **1992**, 114, 705–712.
- [87] D. Shukla, P. Wan, *J. Am. Chem. Soc.* **1993**, 115, 2990–2991.
- [88] P. Wan, D. Shukla, *Chem. Rev.* **1993**, 93, 571–584.
- [89] J. Toldo, O. El Bakouri, M. Solà, P.-O. Norrby, H. Ottosson, *ChemPlusChem* **2019**, 84, 712–721.
- [90] H. Möllerstedt, M. C. Piqueras, R. Crespo, H. Ottosson, *J. Am. Chem. Soc.* **2004**, 126, 13938–13939.
- [91] H. Ottosson, K. Kilså, K. Chajara, M. C. Piqueras, R. Crespo, H. Kato, D. Muthas, *Chem. Eur. J.* **2007**, 13, 6998–7005.
- [92] M. Rosenberg, H. Ottosson, K. Kilså, *Phys. Chem. Chem. Phys.* **2011**, 13, 12912–12919.
- [93] K. Jorner, R. Emanuelsson, C. Dahlstrand, H. Tong, A. V. Denisova, H. Ottosson, *Chem. Eur. J.* **2014**, 20, 9295–9303.
- [94] Y. M. Sung, M.-C. Yoon, J. M. Lim, H. Rath, K. Naoda, A. Osuka, D. Kim, *Nat. Chem.* **2015**, 7, 418–422.
- [95] Y. M. Sung, J. Oh, W. Kim, H. Mori, A. Osuka, D. Kim, *J. Am. Chem. Soc.* **2015**, 137, 11856–11859.
- [96] H. Ottosson, K. E. Borbas, *Nat. Chem.* **2015**, 7, 373–375.
- [97] Y. M. Sung, J. Oh, K. Naoda, T. Lee, W. Kim, M. Lim, A. Osuka, D. Kim, *Angew. Chem. Int. Ed.* **2016**, 55, 11930–11934; *Angew. Chem.* **2016**, 128, 12109–12113.
- [98] R. Breslow, R. Hill, E. Wasserman, *J. Am. Chem. Soc.* **1964**, 86, 5349–5350.
- [99] E. Wasserman, R. S. Hutton, V. J. Kuck, E. A. Chandross, *J. Am. Chem. Soc.* **1974**, 96, 1965–1966.
- [100] C. A. Gould, J. Marbey, V. Vieru, D. A. Marchiori, R. David Britt, L. F. Chibotaru, S. Hill, J. R. Long, *Nat. Chem.* **2021**, 13, 1001–1005.
- [101] K. An, J. Zhu, *J. Organomet. Chem.* **2018**, 864, 81–87.
- [102] R. Papadakis, H. Li, J. Bergman, A. Lundstedt, K. Jorner, R. Ayub, S. Haldar, B. O. Jahn, A. Denisova, B. Zietz, R. Lindh, B. Sanyal, H. Grennberg, K. Leifer, H. Ottosson, *Nat. Commun.* **2016**, 7, 12962.
- [103] H. Kim, W. Park, Y. Kim, M. Filatov, C. H. Choi, D. Lee, *Nat. Commun.* **2021**, 12, 5409.
- [104] M. Ueda, K. Jorner, Y. M. Sung, T. Mori, Q. Xiao, D. Kim, H. Ottosson, T. Aida, Y. Itoh, *Nat. Commun.* **2017**, 8, 346.
- [105] F. A. L. Anet, *J. Am. Chem. Soc.* **1962**, 84, 671–672.
- [106] J. F. M. Oth, *Pure Appl. Chem.* **1971**, 25, 573–622.
- [107] M. Garavelli, F. Bernardi, A. Cembran, O. Castaño, L. M. Frutos, M. Merchán, M. Olivucci, *J. Am. Chem. Soc.* **2002**, 124, 13770–13789.
- [108] R. Ayub, R. Papadakis, K. Jorner, B. Zietz, H. Ottosson, *Chem. Eur. J.* **2017**, 23, 13684–13695.
- [109] W. Adam, R. Finzel, *J. Am. Chem. Soc.* **1992**, 114, 4563–4568.
- [110] P. S. Engel, K. L. Lowe, *Tetrahedron Lett.* **1994**, 35, 2267–2270.
- [111] R. A. Caldwell, L. Zhou, *J. Am. Chem. Soc.* **1994**, 116, 2271–2275.
- [112] G. Bucher, A. A. Mahajan, M. Schmittel, *J. Org. Chem.* **2009**, 74, 5850–5860.

- [113] N. J. Turro, V. Ramamurthy, J. C. Scaiano, *Modern Molecular Photochemistry of Organic Molecules*, University Science Books, Sausalito, 2010.
- [114] J. Zhao, W. Wu, J. Sun, S. Guo, *Chem. Soc. Rev.* **2013**, 42, 5323–5351.
- [115] T. N. Das, K. I. Priyadarsini, *J. Chem. Soc. Faraday Trans.* **1994**, 90, 963–968.
- [116] R. Ayub, K. Jorner, H. Ottosson, *Inorganics* **2017**, 5, 91.
- [117] K.-T. Kang, U. C. Yoon, H. C. Seo, K. N. Kim, H. Y. Song, J. C. Lee, *Bull. Korean Chem. Soc.* **1991**, 12, 57–60.
- [118] T. T. Talele, *J. Med. Chem.* **2016**, 59, 8712–8756.
- [119] M. R. Bauer, P. Di Fruscia, S. C. C. Lucas, I. N. Michaelides, J. E. Nelson, R. I. Storer, B. C. Whitehurst, *RSC Med. Chem.* **2021**, 12, 448–471.
- [120] M. Brink, H. Möllerstedt, C.-H. Ottosson, *J. Phys. Chem. A* **2001**, 105, 4071–4083.
- [121] H. Kato, M. Brink, H. Möllerstedt, M. C. Piqueras, R. Crespo, H. Ottosson, *J. Org. Chem.* **2005**, 70, 9495–9504.
- [122] S. Villaume, H. Ottosson, *J. Phys. Chem. A* **2009**, 113, 12304–12310.
- [123] J. Zhu, H. A. Fogarty, H. Möllerstedt, M. Brink, H. Ottosson, *Chem. Eur. J.* **2013**, 19, 10698–10707.
- [124] J. Zhu, C. Dahlstrand, J. R. Smith, S. Villaume, H. Ottosson, *Symmetry* **2010**, 2, 1653–1682.
- [125] I. Anger, M. Sundahl, O. Wennerström, P. Auchter-Krummel, K. Müllen, *J. Phys. Chem.* **1995**, 99, 650–652.
- [126] M. Baranac-Stojanović, *J. Org. Chem.* **2020**, 85, 4289–4297.
- [127] A. K. Pati, O. El Bakouri, S. Jockusch, Z. Zhou, R. B. Altman, G. A. Fitzgerald, W. B. Asher, D. S. Terry, A. Borgia, M. D. Holsey, J. E. Batchelder, C. Abeywickrama, B. Huddle, D. Rufa, J. A. Javitch, H. Ottosson, S. C. Blanchard, *Proc. Natl. Acad. Sci. USA* **2020**, 117, 24305–24315.
- [128] Y. Inagaki, M. Nakamoto, A. Sekiguchi, *J. Am. Chem. Soc.* **2011**, 133, 16436–16439.
- [129] A. Kostenko, B. Tumanskii, Y. Kobayashi, M. Nakamoto, A. Sekiguchi, Y. Apeloig, *Angew. Chem. Int. Ed.* **2017**, 56, 10183–10187; *Angew. Chem.* **2017**, 129, 10317–10321.
- [130] G. Maier, J. Neudert, O. Wolf, D. Pappusch, A. Sekiguchi, M. Tanaka, T. Matsuo, *J. Am. Chem. Soc.* **2002**, 124, 13819–13826.
- [131] L. A. Paquette, S. V. Ley, R. H. Meisinger, R. K. Russell, M. Oku, *J. Am. Chem. Soc.* **1974**, 96, 5806–5815.
- [132] J. Ostapko, A. Gorski, J. Buczyńska, B. Golec, K. Nawara, A. Kharchenko, A. Listkowski, M. Ceborska, M. Pietrzak, J. Waluk, *Chem. Eur. J.* **2020**, 26, 16666–16675.
- [133] V. T. N. Mai, V. Ahmad, M. Mamada, T. Fukunaga, A. Shukla, J. Sobus, G. Krishnan, E. G. Moore, G. G. Andersson, C. Adachi, E. B. Namdas, S.-C. Lo, *Nat. Commun.* **2020**, 11, 5623.
- [134] R. B. Altman, D. S. Terry, Z. Zhou, Q. Zheng, P. Geggier, R. A. Kolster, Y. Zhao, J. A. Javitch, J. D. Warren, S. C. Blanchard, *Nat. Methods* **2012**, 9, 68–71.
- [135] J. P. Ferris, J. C. Guillemin, *J. Org. Chem.* **1990**, 55, 5601–5606.
- [136] N. Kerisit, C. Rouxel, S. Colombel-Rouen, L. Toupet, J.-C. Guillemin, Y. Trolez, *J. Org. Chem.* **2016**, 81, 3560–3567.
- [137] R. Kotani, L. Liu, P. Kumar, H. Kuramochi, T. Tahara, P. Liu, A. Osuka, P. B. Karadakov, S. Saito, *J. Am. Chem. Soc.* **2020**, 142, 14985–14992.
- [138] T. Yamakado, S. Takahashi, K. Watanabe, Y. Matsumoto, A. Osuka, S. Saito, *Angew. Chem. Int. Ed.* **2018**, 57, 5438–5443.
- [139] Y. Chen, K.-H. Chang, F.-Y. Meng, S.-M. Tseng, P.-T. Chou, *Angew. Chem. Int. Ed.* **2021**, 60, 7205–7212; *Angew. Chem.* **2021**, 133, 7281–7288.
- [140] K. Padberg, J. D. R. Ascherl, F. Hampel, M. Kivala, *Chem. Eur. J.* **2019**, 26, 3474–3478.
- [141] A. Roxin, A. Chase, E. Jeffers, M. Lukeman, *Photochem. Photobiol. Sci.* **2011**, 10, 920–930.
- [142] K. H. Jensen, J. E. Hanson, *Chem. Mater.* **2002**, 14, 918–923.
- [143] M. Reinfelds, J. von Cosel, K. Falahati, C. Hamerla, T. Slanina, I. Burghardt, A. Heckel, *Chem. Eur. J.* **2018**, 24, 13026–13035.
- [144] V. Hermanns, M. Scheurer, N. F. Kersten, C. Abdellaoui, J. Wachtveitl, A. Dreuw, A. Heckel, *Chem. Eur. J.* **2021**, 27, 14121–14127.
- [145] G. Schröder, J. F. M. Oth, *Tetrahedron Lett.* **1966**, 7, 4083–4088.
- [146] T. Slanina, R. Ayub, J. Toldo, J. Sundell, W. Rabten, M. Nicaso, I. Alabugin, I. F. Galván, A. K. Gupta, R. Lindh, A. Orthaber, R. J. Lewis, G. Grönberg, J. Bergman, H. Ottosson, *J. Am. Chem. Soc.* **2020**, 142, 10942–10954.
- [147] D. Bryce-Smith, A. Gilbert, *Tetrahedron* **1976**, 32, 1309–1326.
- [148] I. J. Palmer, I. N. Ragazos, F. Bernardi, M. Olivucci, M. A. Robb, *J. Am. Chem. Soc.* **1993**, 115, 673–682.
- [149] J. Dreyer, M. Klessinger, *Chem. Eur. J.* **1996**, 2, 335–341.
- [150] L. Kaplan, J. S. Ritscher, K. E. Wilzbach, *J. Am. Chem. Soc.* **1966**, 88, 2881–2882.
- [151] E. Farenhorst, A. F. Bickel, *Tetrahedron Lett.* **1966**, 47, 5911–5913.
- [152] B. S. Freiser, J. L. Beauchamp, *J. Am. Chem. Soc.* **1977**, 99, 3214–3225.
- [153] J. Foster, A. L. Pincock, J. A. Pincock, S. Rifai, K. A. Thompson, *Can. J. Chem.* **2000**, 78, 1019–1029.
- [154] J. A. Berson, N. M. Hastry, *J. Am. Chem. Soc.* **1971**, 93, 1549–1551.
- [155] L. Kaplan, D. J. Rausch, K. E. Wilzbach, *J. Am. Chem. Soc.* **1972**, 94, 8638–8640.
- [156] Y. Izawa, H. Tomioka, T. Kagami, T. Sato, *J. Chem. Soc. Chem. Commun.* **1977**, 780–781.
- [157] L. Kaplan, J. W. Pavlik, K. E. Wilzbach, *J. Am. Chem. Soc.* **1972**, 94, 3283–3284.
- [158] U. C. Yoon, S. L. Quillen, P. S. Mariano, R. Swanson, J. L. Stavino, E. Bay, *J. Am. Chem. Soc.* **1983**, 105, 1204–1218.
- [159] S. J. Cho, R. Ling, A. Kim, P. S. Mariano, *J. Org. Chem.* **2000**, 65, 1574–1577.
- [160] F. Glarner, B. Acar, I. Etter, T. Damiano, E. A. Acar, G. Bernardinelli, U. Burger, *Tetrahedron* **2000**, 56, 4311–4316.
- [161] D. W. Cho, P. S. Mariano, *J. Korean Chem. Soc.* **2010**, 54, 261–268.
- [162] J. Zou, P. S. Mariano, *Photochem. Photobiol. Sci.* **2008**, 7, 393–404.
- [163] K. Wakita, N. Tokitoh, R. Okazaki, N. Takagi, S. Nagase, *J. Am. Chem. Soc.* **2000**, 122, 5648–5649.
- [164] M.-D. Su, *Organometallics* **2014**, 33, 5231–5237.
- [165] H. Ottosson, A. M. Eklöf, *Coord. Chem. Rev.* **2008**, 252, 1287–1314.
- [166] M. F. Rode, A. L. Sobolewski, C. Dedonder, C. Jouvet, O. Dopfer, *J. Phys. Chem. A* **2009**, 113, 5865–5873.
- [167] S. Winstein, *J. Am. Chem. Soc.* **1959**, 81, 6524–6525.
- [168] R. F. Childs, *Acc. Chem. Res.* **1984**, 17, 347–352.
- [169] R. V. Williams, *Chem. Rev.* **2001**, 101, 1185–1204.
- [170] J. I. Brauman, J. Schwartz, E. E. van Tamelen, *J. Am. Chem. Soc.* **1968**, 90, 5328–5329.
- [171] J. Schwartz, *J. Chem. Soc. D* **1969**, 833–834.
- [172] K. Jorner, B. O. Jahn, P. Bultinck, H. Ottosson, *Chem. Sci.* **2018**, 9, 3165–3176.
- [173] V. Vijay, M. Madhu, R. Ramakrishnan, A. Benny, M. Hariharan, *Chem. Commun.* **2020**, 56, 225–228.
- [174] A. Krishnan, A. Diaz-Andres, K. P. Sudhakaran, A. T. John, M. Hariharan, D. Casanova, *J. Phys. Org. Chem.* **2023**, 36, e4438.
- [175] G. Markert, E. Paenurk, R. Gershoni-Poranne, *Chem. Eur. J.* **2021**, 27, 6923–6935.
- [176] R. Pino-Rios, R. Báez-Grez, M. Solà, *Phys. Chem. Chem. Phys.* **2021**, 23, 13574–13582.
- [177] N. C. Baird, *J. Phys. Org. Chem.* **2023**, 36, e4459.
- [178] C. Nitu, S. Crespi, *J. Phys. Org. Chem.* **2023**, 36, e4437.
- [179] A. Desvals, S. A. Baudron, V. Bulach, N. Hoffmann, *J. Org. Chem.* **2021**, 86, 13310–13321.
- [180] A. Weller, *Z. Phys. Chem.* **1958**, 15, 438–453.
- [181] Z. Wen, L. J. Karas, C.-H. Wu, J. I.-C. Wu, *Chem. Commun.* **2020**, 56, 8380–8383.
- [182] I. León, J. A. Fernández, *J. Chem. Phys.* **2019**, 150, 214306.
- [183] D. J. M. Lyons, C. Empel, D. P. Pace, A. H. Dinh, B. K. Mai, R. M. Koenigs, T. V. Nguyen, *ACS Catal.* **2020**, 10, 12596–12606.
- [184] P. Wan, D. W. Brousmiche, C. Z. Chen, J. Cole, M. Lukeman, M. Xu, *Pure Appl. Chem.* **2001**, 73, 529–534.
- [185] B. J. Lampkin, Y. H. Nguyen, P. B. Karadakov, B. Vanveller, *Phys. Chem. Chem. Phys.* **2019**, 21, 11608–11614.
- [186] C. H. Wu, L. J. Karas, H. Ottosson, J. I. C. Wu, *Proc. Natl. Acad. Sci. USA* **2019**, 116, 20303–20308.
- [187] L. D. Mena, D. M. A. Vera, M. T. Baumgartner, *RSC Adv.* **2020**, 10, 39049–39059.
- [188] E. M. Arpa, B. Durbreej, *Phys. Chem. Chem. Phys.* **2022**, 24, 11496–11500.
- [189] N. Nishina, T. Mutai, J. Aihara, *J. Phys. Chem. A* **2017**, 121, 151–161.
- [190] L. Gutiérrez-Arzaluz, F. Cortés-Guzmán, T. Rocha-Rinza, J. Peón, *Phys. Chem. Chem. Phys.* **2015**, 17, 31608–31612.
- [191] Đ. Škalamera, C. Bohne, S. Landgraf, N. Basarić, *J. Org. Chem.* **2015**, 80, 10817–10828.
- [192] J. Ma, M. Šekutor, Đ. Škalamera, N. Basarić, D. L. Phillips, *J. Org. Chem.* **2019**, 84, 8630–8637.
- [193] Đ. Škalamera, I. Antol, K. Mlinarić-Majerski, H. Vančik, D. L. Phillips, J. Ma, N. Basarić, *Chem. Eur. J.* **2018**, 24, 9426–9435.
- [194] R. H. Mitchell, Y. Chen, *Tetrahedron Lett.* **1996**, 37, 5239–5242.
- [195] R. H. Mitchell, *Eur. J. Org. Chem.* **1999**, 1999, 2695–2703.
- [196] Y. Yang, Y. Xie, Q. Zhang, K. Nakatani, H. Tian, W. Zhu, *Chem. Eur. J.* **2012**, 18, 11685–11694.

- [197] H. Löfås, B. O. Jahn, J. Wärnå, R. Emanuelsson, R. Ahuja, A. Grigoriev, H. Ottosson, *Faraday Discuss.* **2014**, *174*, 105–124.
- [198] V. Lovrinčević, D. Vuk, I. Škorić, N. Basarić, *J. Org. Chem.* **2022**, *87*, 2489–2500.
- [199] D. Halder, A. K. Ray, A. Paul, *J. Phys. Org. Chem.* **2023**, *36*, e4456.
- [200] M. Irie, M. Mohri, *J. Org. Chem.* **1988**, *53*, 803–808.
- [201] S. Nakamura, M. Irie, *J. Org. Chem.* **1988**, *53*, 6136–6138.
- [202] B. Oruganti, P. Pál Kalapos, V. Bhargav, G. London, B. Durbeej, *J. Am. Chem. Soc.* **2020**, *142*, 13941–13953.
- [203] D. Kitagawa, T. Nakahama, Y. Nakai, S. Kobatake, *J. Mater. Chem. C* **2019**, *7*, 2865–2870.
- [204] B. Oruganti, J. Wang, B. Durbeej, *J. Org. Chem.* **2022**, *87*, 11565–11571.
- [205] R. K. Mohamed, S. Mondal, K. Jorner, T. F. Delgado, V. V. Lobodin, H. Ottosson, I. V. Alabugin, *J. Am. Chem. Soc.* **2015**, *137*, 15441–15450.
- [206] A. Banerjee, D. Halder, G. Ganguly, A. Paul, *Phys. Chem. Chem. Phys.* **2016**, *18*, 25308–25314.
- [207] D. Halder, A. Paul, *J. Phys. Chem. A* **2020**, *124*, 3976–3983.
- [208] R. Schmidt, D. Geissler, V. Hagen, J. Bendig, *J. Phys. Chem. A* **2007**, *111*, 5768–5774.
- [209] R. S. Givens, M. Rubina, J. Wirz, *Photochem. Photobiol. Sci.* **2012**, *11*, 472–488.
- [210] J. Kim, H. Kim, J. Oh, D. Kim, *Bull. Korean Chem. Soc.* **2022**, *43*, 508–513.
- [211] J. Oh, Y. M. Sung, H. Mori, S. Park, K. Jorner, H. Ottosson, M. Lim, A. Osuka, D. Kim, *Chem* **2017**, *3*, 870–880.
- [212] L. J. Karas, C.-H. Wu, H. Ottosson, J. I. Wu, *Chem. Sci.* **2020**, *11*, 10071–10077.
- [213] D. Rehm, A. Weller, *Isr. J. Chem.* **1970**, *8*, 259–271.
- [214] S. Farid, J. P. Dinnocenzo, P. B. Merkel, R. H. Young, D. Shukla, G. Guirado, *J. Am. Chem. Soc.* **2011**, *133*, 11580–11587.
- [215] K. Jorner, W. Rabten, T. Slanina, N. Proos Vedin, S. Sillén, J. Wu Ludvigsson, H. Ottosson, P.-O. Norrby, *Cell Rep. Phys. Sci.* **2020**, *1*, 100274.
- [216] H. I. Hamoudi, P. F. Heelis, R. A. Jones, S. Navaratnam, B. J. Parsons, G. O. Phillips, M. J. Vandenburg, W. J. C. Currie, *Photochem. Photobiol.* **1984**, *40*, 35–39.
- [217] D. E. Moore, in *Drugs Photochem. Photostability* (Eds.: E. Albin, A. Fasani), Royal Society of Chemistry, Cambridge, **1998**, 100–115.
- [218] Y. N. Li, D. E. Moore, B. N. Tattam, *Int. J. Pharm.* **1999**, *183*, 109–116.
- [219] P. Calza, C. Massolino, G. Monaco, C. Medana, C. Baiocchi, *J. Pharm. Biomed. Anal.* **2008**, *48*, 315–320.
- [220] H. H. Tønnesen, *Photostability of Drugs and Drug Formulations*, CRC Press, **2004**.
- [221] S. Walia, P. Dureja, S. K. Mukerjee, *Arch. Environ. Contam. Toxicol.* **1988**, *17*, 183–188.
- [222] T. Keijer, V. Bakker, J. C. Slootweg, *Nat. Chem.* **2019**, *11*, 190–195.

Manuscript received: November 30, 2022
Accepted manuscript online: January 30, 2023
Version of record online: February 24, 2023